Journal of Medicinal Chemistry

Article

Cite This: J. Med. Chem. 2019, 62, 3971−3988

pubs.acs.org/jmc

Discovery of Potent Myeloid Cell Leukemia-1 (Mcl-1) Inhibitors That Demonstrate in Vivo Activity in Mouse Xenograft Models of Human Cancer

Taekyu Lee,[†] Plamen P. Christov,[‡] Subrata Shaw,[†,◆] James C. Tarr,[†] Bin Zhao,[†] Nagarathanam Veerasamy,[†] Kyu Ok Jeon,[†] Jonathan J. Mills,[†] Zhiguo Bian,[†,¶] John L. Sensintaffar,[†] Allison L. Arnold,[†] Stuart A. Fogarty,[†,●] Evan Perry,[†] Haley E. Ramsey,[§] Rebecca S. Cook,[∥] Melinda Hollingshead,[#] Myrtle Davis Millin,[#,⋈] Kyung-min Lee,[⊥,⋈] Brian Koss,[▽,⧖] Amit Budhraja,[▽] Joseph T. Opferman,[▽] Kwangho Kim,[‡] Carlos L. Arteaga,[⊥,⋈] William J. Moore,[○] Edward T. Olejniczak,[†] Michael R. Savona,[§] and Stephen W. Fesik*[,†]

[†]Department of Biochemistry, Vanderbilt University School of Medicine, 2215 Garland Avenue, 607 Light Hall, Nashville, Tennessee 37232-0146, United States

[‡]Chemical Synthesis Core, Vanderbilt Institute of Chemical Biology, Vanderbilt University, Nashville, Tennessee 37232, United States

[§]Department of Medicine, Vanderbilt-Ingram Cancer Center, Nashville, Tennessee 37232, United States

[∥]Department of Cell and Developmental Biology, Vanderbilt University School of Medicine, Nashville, Tennessee 37232, United States

[⊥]Department of Hematology and Oncology, Vanderbilt University School of Medicine, Nashville, Tennessee 37232, United States

[#]National Cancer Institute, Bethesda, Maryland 20892, United States

[▽]Department of Cell and Molecular Biology, St. Jude Children's Research Hospital, Memphis, Tennessee 38105, United States

[○]Leidos Biomedical Research, Frederick National Laboratory for Cancer Research, Frederick, Maryland 21701, United States

Supporting Information

ABSTRACT: Overexpression of myeloid cell leukemia-1 (Mcl-1) in cancers correlates with high tumor grade and poor survival. Additionally, Mcl-1 drives intrinsic and acquired resistance to many cancer therapeutics, including B cell lymphoma 2 family inhibitors, proteasome inhibitors, and antitubulins. Therefore, Mcl-1 inhibition could serve as a strategy to target cancers that require Mcl-1 to evade apoptosis. Herein, we describe the use of structure-based design to discover a novel compound (**42**) that robustly and specifically inhibits Mcl-1 in cell culture and animal xenograft models. Compound **42** binds to Mcl-1 with picomolar affinity and inhibited growth of Mcl-1-dependent tumor cell lines in the nanomolar range. Compound **42** also inhibited the growth of hematological and triple negative breast cancer xenografts at well-tolerated doses. These findings highlight the use of structure-based design to identify small molecule Mcl-1 inhibitors and support the use of **42** as a potential treatment strategy to block Mcl-1 activity and induce apoptosis in Mcl-1-dependent cancers.

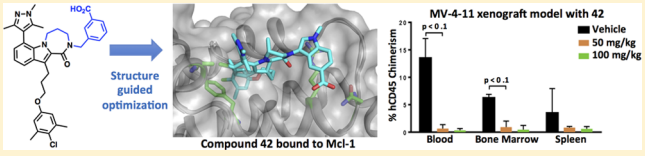

INTRODUCTION

To evade the normal response to severe stress, many cancer cell types possess a defect in the signal transduction of programmed cell death (apoptosis).[1−4] The B cell lymphoma 2 (Bcl-2) family of proteins are key regulators of apoptosis and are often deregulated in numerous diseases, including cancer.[2,5−8] Improper regulation of Bcl-2 family members can increase the threshold for apoptosis, thus allowing cancer cells to survive under conditions that normal cells would sense as aberrant and respond by inducing apoptosis.[1,3,4] The Bcl-2 family of proteins is comprised of antiapoptotic (Bcl-2, Bcl-xL, Bcl-w, Bcl-A1, and myeloid cell leukemia-1 (Mcl-1)) and proapoptotic (Bim, Bid, Bad, PUMA, NOXA, Bak, Bax) members. Antiapoptotic Bcl-2 family members bind to and sequester proapoptotic proteins and thereby prevent Bak/Bax oligiomerization, permeabilization of the outer mitochondrial membrane, and the commitment of the cell to undergo apoptosis.[1,2,5,6] Amplification of the gene encoding the antiapoptotic protein Mcl-1 is one of the most common genetic aberrations in human cancer, and Mcl-1 is frequently overexpressed in hematologic, breast, and lung cancers.[8−18] Importantly, Mcl-1 overexpression contributes to therapeutic resistance to several cancer treatments, including vincristine,

Received: December 19, 2018
Published: March 30, 2019

DOI: 10.1021/acs.jmedchem.8b01991
J. Med. Chem. 2019, 62, 3971−3988

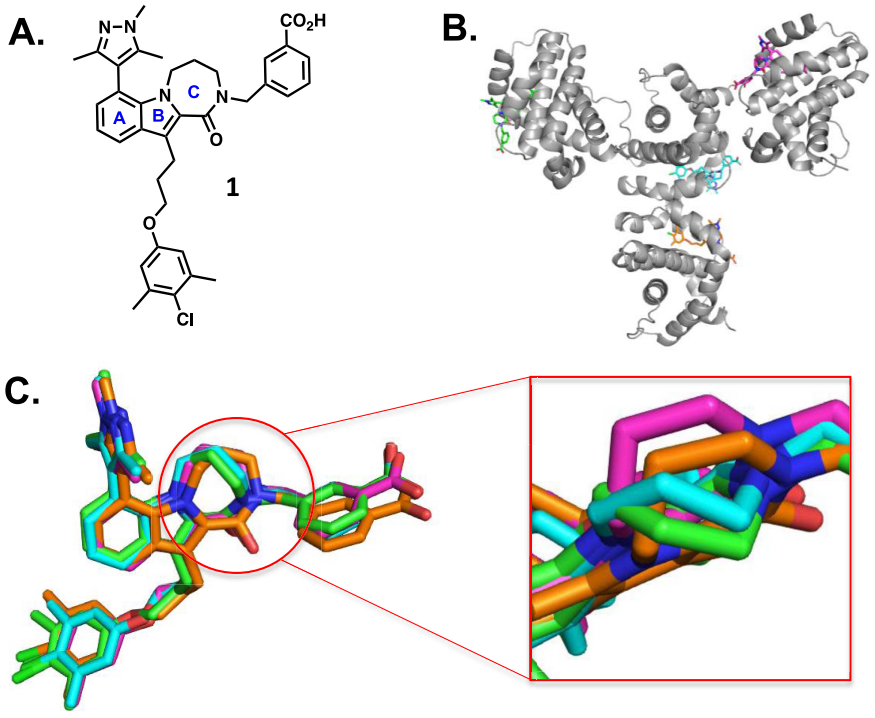

Figure 1. (A) Structure of tricyclic diazepinone Mcl-1 inhibitor (**1**). (B) Asymmetric unit contains four copies of Mcl-1 (gray)/ligand (**1**) (green, cyan, magenta, and orange) complex (6BW2). (C) Overlay of each copy of Mcl-1 inhibitor from the asymmetric unit illustrating similarity in binding pose of indole core, benzyl amide, propoxyphenyl ether, and trimethyl pyrazole and expansion highlighting variation in the binding pose of diazepinone ring.

taxol, gemcitabine, cisplatin, and others.[19,20] Therapeutic resistance can, however, be reversed through down-regulation of Mcl-1 by RNA interference, illustrating the therapeutic potential for targeting Mcl-1 inhibition for the treatment of cancer.[6,7,20,21]

Bcl-2 family members possess a conserved Bcl-2 homology 3 (BH3) domain, which is central to the apoptotic function of proteins in this family. The BH3 domain binds to four hydrophobic pockets (P1−P4) of the antiapoptotic members of the Bcl-2 family, including Mcl-1, thus sequestering the BH3-containing apoptotic protein and preventing its ability to activate apoptosis. BH3 domains consist of an amphipathetic α-helix containing four hydrophobic residues which bind to P1−P4 within the antiapoptotic proteins.[4,22−25] A small molecule inhibitor capable of displacing the BH3-containing proapoptotic protein from the antiapoptotic family member could restore apoptotic signaling within a cancer cell. One challenge in disrupting this interaction is the high binding affinity between Bcl-2 family members resulting from a large protein−protein interaction.[26] Inhibiting this interaction requires molecules with very high binding affinity in the picomolar range.[27] This strategy of inducing apoptosis with a small molecule inhibitor of the antiapoptotic Bcl-2 family of proteins was validated by the Food and Drug Administration's approval of Venetoclax, a Bcl-2 selective inhibitor for the treatment of chronic lymphocytic leukemia.[28−30]

Recently, a number of Mcl-1 selective inhibitors have been described.[31−37] One of the most promising compounds, S63845, has shown robust activity in multiple Mcl-1 sensitive cell lines and achieved single agent activity in animal xenograft models of human hematological cancers.[38] This compound, and others described in the patent literature, have targeted the antiapoptotic protein Mcl-1 to trigger apoptosis in cancer cells while maintaining a therapeutic window to minimally affect normal cells. We have previously reported the discovery of potent Mcl-1 inhibitors,[39−44] starting from an initial 2-indole carboxylic acid lead compound[40] and progressing to a series bearing a novel tricyclic-fused indole diazepinone core unit via structure-based design.[39] In addition to potently inhibiting Mcl-1, these compounds showed desirable pharmaceutical properties, such as good passive permeability and aqueous solubility, allowing them to deliver robust and selective antiproliferative activities in Mcl-1 sensitive cell lines in a dose-dependent manner. Although these compounds were able to demonstrate sub-nanomolar binding affinities, further improvement in the cellular efficacy was necessary to achieve in vivo efficacy. However, the most promising compound identified within this series (ref 39, compound **39**) suffered from high clearance, low exposure, and a short half-life in rat (intravenous (IV) dosing, 1 mg/kg: CL = 245 mL/min/kg, AUC = 67 nM·h, $t_{1/2}$ = 0.57 h), precluding its advancement to in vivo efficacy studies.

Herein, we report our continued efforts to develop a potent and selective Mcl-1 inhibitor that builds upon our recently reported tricyclic amide series.[39] Structural modifications to this series guided by structure-based design have resulted in ligands that bind to Mcl-1 with low picomolar binding affinity. The compounds reported in this work demonstrate antiproliferative activity in Mcl-1-dependent cell lines, exert their effect through on-target inhibition of Mcl-1, and display efficacy in animal xenograft models of hematological and breast cancers.

RESULTS AND DISCUSSION

Reducing Conformational Flexibility in Diazepinone Core. To further improve upon the potency and pharmaco-

DOI: 10.1021/acs.jmedchem.8b01991
J. Med. Chem. 2019, 62, 3971−3988

Table 1. Binding Affinity of Diazepinone Lactam Tricycles

R		K_i (nM)	1% FBS[a]	K_i (nM)	1% FBS	K_i (nM)	1% FBS	K_i (nM)	1% FBS
H		12±2	101±20	43±3	>200	42±2	150±50	70±30	>200
		2		**6**		**7**		**11**	
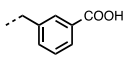		4.9±2	18			11±6	144±60	12±3	>200
		3				**8**		**12**	
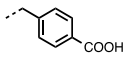		3.3±0.6	3.8			7.1±3	22±7	6.6±3	42±1
		4				**9**		**13**	
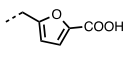		2.9±0.1	27±0.7			7.6±6	81±30	8.2±7	120±60
		5				**10**		**14**	

[a]Mcl-1 K_i in the presence of 1% fetal bovine serum.

Table 2. Binding Affinity of Piperazinone Lactam Tricycles

R		K_i (nM)	1% FBS[a]	K_i (nM)	1% FBS	K_i (nM)	1% FBS	K_i (nM)	1% FBS	Ki (nM)	1% FBS
H		35	>200	47±40	195±7	15	67±40	27±5	151±70	73±10	145±1
		15		**19**		**23**		**27**		**31**	
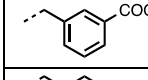		9.6±2	52±10	37±5	170±40	1.1±0.4	26±7	2.1±0.7	67±40	9.9±2	97±3
		16		**20**		**24**		**28**		**32**	
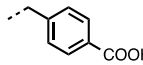		7.2±4	51±3	35±7	191±10	0.77±0.01	6.7±3	1.8±0.07	53±50	9.6±0.5	54±20
		17		**21**		**25**		**29**		**33**	
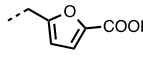		5.8±0.1	137±70	22±9	193±8	1.0±0.03	26±8	5.9±0.6	39±20	8.7±0.7	150±40
		18		**22**		**26**		**30**		**34**	

[a]Mcl-1 K_i in the presence of 1% fetal bovine serum.

kinetic profile of our tricyclic diazepinone series, we sought to optimize the three-carbon linker portion of the diazepinone. This region of the diazepinone ring allowed for significant conformational flexibility, as evidenced by multiple conformations of this moiety in X-ray co-crystal structures of compound **1** with Mcl-1 (Figure 1). This conformational flexibility of the diazepinone ring can also impact the exit vector of the amide substituent and affect the binding pose of the key carboxylic acid moiety. To restrict the conformational freedom of the diazepinone C-ring, we envisioned either the introduction of a methyl group at the 5, 6, or 7-postion or replacement of the diazepinone ring with a six-membered piperazinone ring. To determine the effects of each modification to the core, the binding affinities of the unsubstituted lactam core and three representative benzyl amides for each C-ring modification were compared in a fluorescence polarization assay (FPA), a binding assay, both with and without the presence of 1% fetal bovine serum (FBS) as an assessment of plasma protein binding. The benzyl amides were selected for consistency of comparison with **1**, ease of synthesis, and to afford products with a binding affinity to Mcl-1 within the range that could be easily evaluated in the FPA assay.

A set of analogues bearing a racemic methyl substituent introduced at the 5-, 6-, and 7-positions of the diazepinone ring was synthesized (Table 1). Methylation at the 5-position (**6**) led to a reduction in binding affinity in the NH lactam core, and the increased steric hindrance at this diazepinone position resulted in a low chemical yield of **6**, precluding the synthesis of benzyl amides for this modification. Introduction of a methyl substituent at either the 6- (**7**−**10**) or 7-position (**11**−**14**) of the diazepinone ring resulted in modest losses (2−3-fold) of binding affinity as compared to the unsubstituted diazepinone in the absence of FBS. In the presence of 1% FBS, this effect was more pronounced, with decreases in binding affinity between 3- and 8-fold being observed.

Optimization of Tricyclic Piperazinone Core. With the lack of improvement in the binding affinity from modifications to the diazepinone ring, the effects of replacing the diazepinone ring with a six-membered piperazinone tricyclic core were explored. A set of compounds containing the same

DOI: 10.1021/acs.jmedchem.8b01991
J. Med. Chem. 2019, 62, 3971−3988

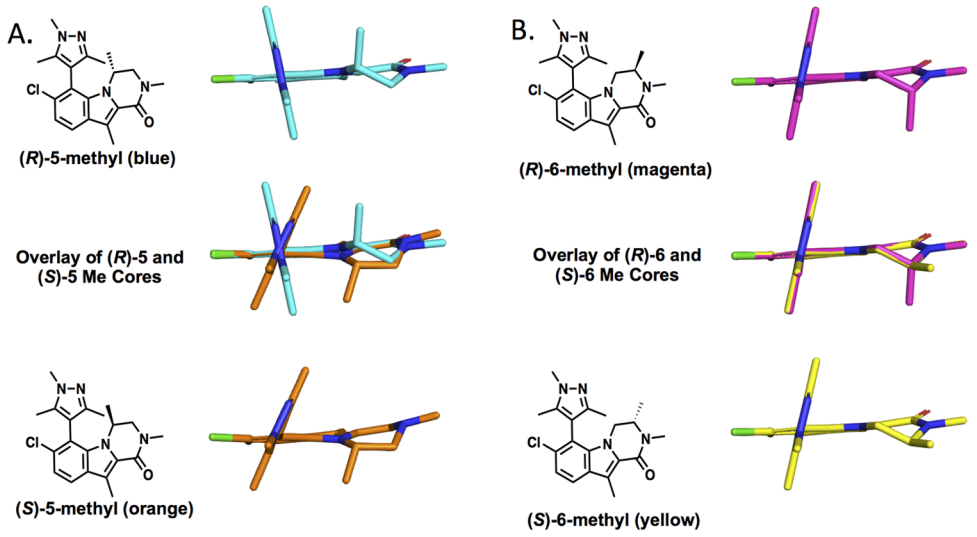

Figure 2. (A) Overlay of energy-minimized conformation of (*R*)-5-methyl piperazinone core (blue) and (*S*)-5-methyl piperazinone core (orange). (B) Overlay of energy-minimized conformation of (*R*)-6-methyl piperazinone core (magenta) and (*S*)-6-methyl piperazinone core (yellow).

Table 3. TR-FRET Binding Affinity of Compounds to Mcl-1, Bcl-xL, and Bcl-2

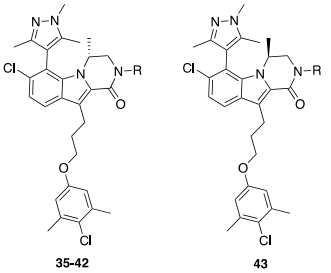

35-42 43

Comp.	R	K_i (nM) TR-FRET		GI_{50} (μM)		Caspase3/7 EC_{50} (μM) H929	K_i (μM) FPA	
		Mcl-1	1% FBS[a]	H929	K562		Bcl-xL	Bcl-2
35		1.4±0.3	2.6+0.7	4.4±0.01	>12.5	3.1±1.5	>40	0.99±0.05
36		1.3±0.2	4.5+0.3	4.0±0.1	>12.5	2.8±1	>40	0.69±0.06
37		0.21±0.003	1.5+0.08	0.82±0.01	>12.5	0.91±0.4	>40	0.77±0.05
38		1.3±0.4	6.8±0.4	2.1±0.2	>12.5	2.2±0.6	>40	0.63±0.1
39		0.42±0.1	1.4±0.5	1.7±0.1	>12.5	0.95±0.4	25±7	0.63±0.07
40		0.33±0.1	0.77±0.1	0.65±0.1	2.5±0.2	0.66±0.2	26±8	0.38±0.05
41		0.081±0.01	0.38±0.01	0.29±0.07	>12.5	0.34±0.1	>40	0.50±0.3
42		0.030±0.02	0.25±0.004	0.19±0.03	9.3±4	0.16±0.07	>40	0.73±0.1
***P*-42**		0.058±0.010	0.18±0.01	0.12±0.01	9.2±5	0.13±0.05	>40	1.3±0.2
***M*-42**		0.058±0.03	0.19±0.02	0.12±0.02	9.2±2	0.11±0.2	>40	1.3±0.3
43		1.6±0.3	6.1±0.7	3.6±0.1	>12.5	2.8±1	--	--

[a]Mcl-1 K_i in the presence of 1% fetal bovine serum.

representative benzyl amides was synthesized to evaluate the effects on the binding affinity of the introduction of unsubstituted and methylated piperazinones to the tricyclic core unit (Table 2). In contrast to the diazepinone series, we were able to readily synthesize each methylated piperazinone enantiomer separately, allowing the effects of the stereochemistry of the methyl substituent to be examined. The unsubstituted piperazinone derivatives (**15**–**18**) exhibited

DOI: 10.1021/acs.jmedchem.8b01991
J. Med. Chem. 2019, 62, 3971−3988

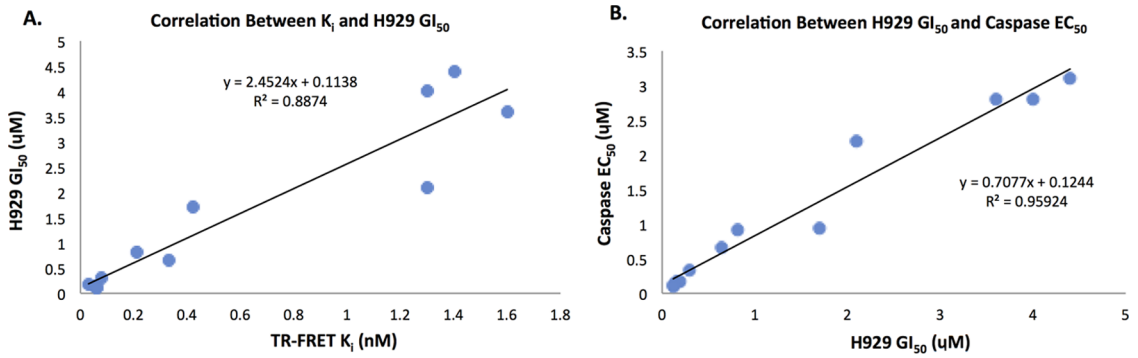

Figure 3. (A) Correlation between binding affinity and H929 GI_{50} in the growth inhibition assay. (B) Correlation between H929 GI_{50} in growth inhibition assay and caspase activation EC_{50}.

weaker binding affinity to Mcl-1 than the unsubstituted diazapinone analogues, both in the absence and presence of 1% FBS. Introduction of an (*R*)-methyl group at the 5-position (**23**−**26**) of the piperazinone ring resulted in a 5−10-fold improvement in binding affinity relative to the unsubstituted piperazinone, whereas introduction of a (*S*)-methyl group (**19**−**22**) resulted in a 3−5-fold loss in binding affinity, resulting in up to a 30-fold difference in binding between the eutomer and distomer. Introduction of a (*R*)-methyl group at the 6-position of the piperazinone ring provided a modest increase in binding affinity relative to the unsubstituted ring (up to 4-fold), and the (*S*)-6-methyl group showed no significant changes relative to the unsubstituted piperazinone. For methylation at both the 5- and 6-positions of the piperazinone ring, the difference in binding affinities of the eutomer/distomer was less pronounced in the presence of 1% FBS.

The impact of the methyl stereochemistry on the binding affinity was further evaluated by performing an energy minimization calculation for each pair of enantiomeric methyl substituents on a simplified tricyclic piperazinone core using Maestro Ligand 2D Workspace (Figure 2). Substitution of the piperazinone 6-position with either an (*R*)- or (*S*)-methyl group had a minimal impact on the dihedral angle between the trimethyl pyrazole and indole rings, which is in agreement with the modest effect of the methyl stereochemistry at this site (Figure 2B). Introduction of a methyl group at the 5-position, however, had a dramatic impact on the dihedral angle between the trimethyl pyrazole and indole rings due to steric repulsion between the piperazinone methyl group and the trimethyl pyrazole as well as subtle effect on the exit vector of the amide substituent, which may justify the larger difference in binding affinities observed for the two enantiomers. These results suggest that the lowest energy conformation of (*R*)-5-methyl piperazinone core may be similar to that adopted by the inhibitors when bound to Mcl-1.

Optimization of (*R*)-5-Methyl Piperazinone Aryl Amide Inhibitors. With the optimized (*R*)-5-methyl piperazinone-containing core in hand, the effect of different amide substituents at the N1 position of the piperazinone was examined. As described in our discovery of the tricyclic diazepinone series, electron-rich-fused bicyclic amide substituents efficiently engage in a cation−π interaction with R263; resulting in improved binding affinity and efficacy in cellular growth inhibition assays. Starting from the tricyclic (*R*)-5-methyl piperazinone core, a library (**35**−**43**) containing the most promising *N*-aryl and *N*-heteroaryl substituents identified from the tricyclic diazepinone series[39] was prepared and evaluated in the time-resolved fluorescence energy transfer (TR-FRET) binding assay in the presence and absence of 1% FBS and a cellular growth inhibition assay using Mcl-1 sensitive multiple myeloma cell line H929 and Mcl-1 insensitive cell line K562 to evaluate off-target liabilities (Table 3). Compounds bearing a single phenyl ring (**35** and **36**) displayed a 5−10-fold improvement in the binding affinity compared to benzyl amides **24**−**26** in the presence of 1% FBS, however, in the absence of FBS displayed comparable binding affinities. These data suggest that the aryl amide series reduces the degree of plasma protein binding relative to the benzyl amide series. Introduction of bicyclic aryl groups led to compounds with even further enhanced Mcl-1 binding affinities, with several analogues exhibiting picomolar binding affinity. As expected, electron-rich bicyclic aryl rings proved to be most potent as they enhanced the cation−π interaction between the aryl group and R263. The most potent compound identified in the binding assay, **42**, exhibited K_i = 70 and 300 pM in the absence and presence of 1% FBS, respectively. The excellent binding affinity of **42** translated into potent cellular activity, achieving a GI_{50} in H929 cells of 190 nM. Due to hindered rotation between the trimethyl pyrazole and indole rings, compound **42** exists as a mixture of diastereomeric atropisomers. These compounds were separable by high-performance liquid chromatography (HPLC) and found to possess similar binding affinities. The (*S*)-5-methyl piperazinone analogue **43** was prepared as a negative control and found to exhibit a 50-fold weaker binding affinity compared to **42**, consistent with the trend observed for **19**−**22**. The structure of **42**, and its evaluation in xenograft models of human hematological cancers, has been previously reported by Ramsey et al.[44]

In addition to the potent binding to Mcl-1, the compounds also maintained a high selectivity toward other Bcl-2 family members. Binding to Bcl-2 and Bcl-xL was 10^4- and 10^7-fold weaker, respectively. Within this series, there was an excellent correlation between the observed binding affinities and cellular efficacy (Figure 3A), providing evidence that these compounds exert their effects through binding to Mcl-1. To further establish the on-target mechanism of action of these compounds, the caspase activation was measured in H929 cells and found to correlate closely with the observed GI_{50} (Figure 3B).

X-ray Co-crystal Structure of 42 Bound to Mcl-1. To understand how **42** achieves its high affinity, the X-ray co-crystal structure of **42** bound to Mcl-1 was obtained (Figure

DOI: 10.1021/acs.jmedchem.8b01991
J. Med. Chem. 2019, 62, 3971−3988

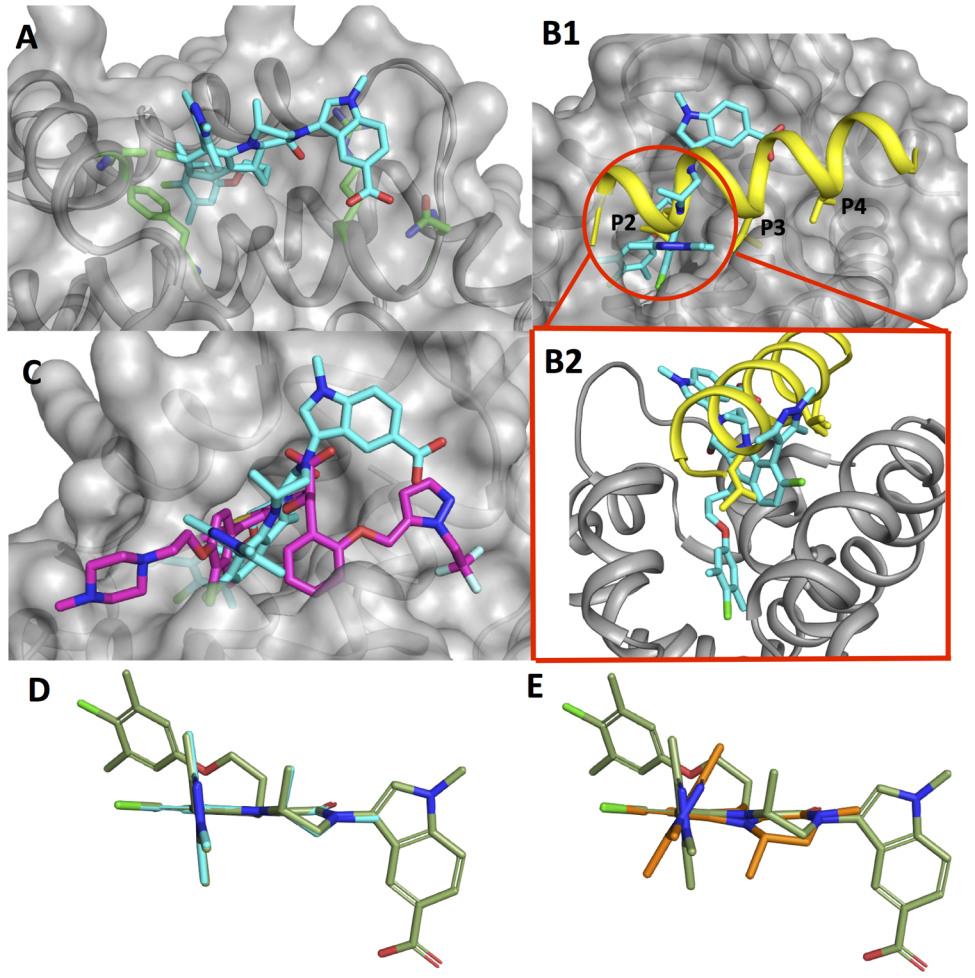

Figure 4. (A) X-ray co-crystal structure of Mcl-1 inhibitor **42** (cyan) and Mcl-1 (6NE5). (B1) Overlay of Mcl-1 inhibitor **42** (cyan) and 16-mer (yellow) derived from Mcl-1 BH3 region (4HW4). (B2) Comparison of depth of ligand in P2 pocket of inhibitor **42** and 16-mer. (C) Overlay of Mcl-1 inhibitors **42** (cyan) and S63854 (magenta) (5LOF).[38] (D) Overlay of (*R*)-5-methyl piperazinone tricyclic core (cyan) with X-ray co-crystal structure of compound **42** (olive) and Mcl-1. (E) Overlay of (*S*)-5-methyl piperazinone tricyclic core (orange) with X-ray co-crystal structure of compound **42** (olive) and Mcl-1.

4A). In Figure 4B, the X-ray co-crystal structure of **42** binding to Mcl-1 is compared to that of a 16-mer peptide derived from the BH3 domain of Mcl-1. It can be seen that although **42** still lies in the peptide binding groove, it exploits different contacts to the protein than the peptides. For example, the dimethyl-chlorophenyl ether of **42** goes much deeper into the P2 hydrophobic pocket than the leucine present in BH3-only members of the Bcl-2 family of proteins. It can also be seen that compound **42** does not fully occupy P3, with only the methyl of the trimethyl pyrazole pointing toward this pocket, nor does the compound reach as far as the peptide P4 pocket which is exploited by S63845, another Mcl-1 inhibitor (Figure 4C).[38] However, compound **42** does make an important contact with the protein (Figure 4A) by using the indole headpiece to cover R263, generating a pseudo-hydrophobic pocket around this residue. Shielding this hydrophilic residue from solvent results in a significant gain in affinity due to the desolvation of the protein ligand interface. Additionally, the indole headpiece also positions the carboxylic acid to make a favorable H-bonding interaction with Asn 260 to further stabilize the complex. Thus, three different classes of Mcl-1 inhibitors (peptides, piperazinone amides series, S63845 series) are all able to achieve high binding affinity to Mcl-1; however, each class of compounds adopts a distinct binding pose and utilizes novel interactions within the binding groove.

The X-ray co-crystal structure of **42** also provides further insight to the tighter binding affinity observed for the (*R*)-5-methyl piperazinone as compared to the (S) enantiomer. Overlaying the energy-minimized conformations of the (*R*)- and (*S*)-5-methyl piperizinone tricyclic lactam cores (Figure 2) with the X-ray structure of **42** bound to Mcl-1 shows that the energy-minimized conformation of the (R) enantiomer (eutomer) aligns very closely to the observed binding pose of **42** (Figure 4D). In the overlay of the energy-minimized conformation of the (*S*)-methyl piperazinone core (distomer) with **42**, however, the pyrazole ring is significantly distorted from the binding pose observed for **42** due to the steric repulsion between the (*S*)-methyl group and the trimethyl pyrazole.

In Vitro Cell Line Experiments Demonstrate On-Target Activity. The on-target Mcl-1 activity of **42** was characterized using multiple in vitro cell line experiments. Co-immunoprecipitation (Co-IP) experiments of Mcl-1, Bcl-xL, and Bim in the NCI-H929 cell line indicate that dosing with compound **42** causes the mechanism-based dose-dependent displacement of Bim from Mcl-1 (Figure 5A) that is expected

DOI: 10.1021/acs.jmedchem.8b01991
J. Med. Chem. 2019, 62, 3971−3988

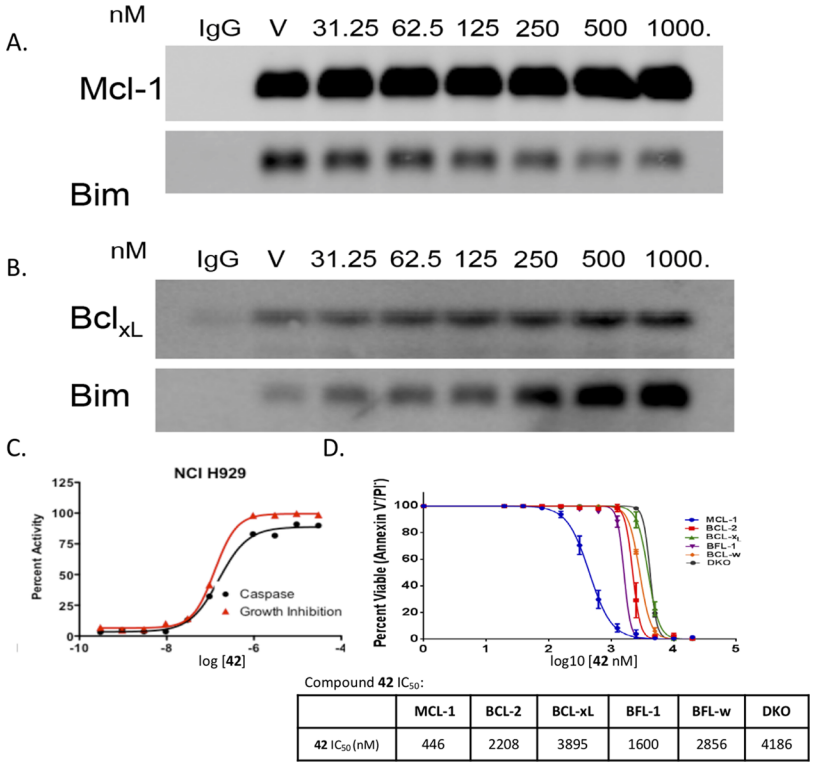

Compound **42** IC_{50}:

	MCL-1	BCL-2	BCL-xL	BFL-1	BFL-w	DKO
42 IC_{50} (nM)	446	2208	3895	1600	2856	4186

Figure 5. Cell line on-target activity studies with **42**. (A, B) Co-IP experiments showing Bim complexation as a function of **42** dosed in H929 cells. (A) Co-IP of Mcl-1 and Bim, (B) Bcl-xL and Bim, vehicle control V was treated with 0.1% dimethyl sulfoxide (DMSO). (C) Comparison of dose-dependent changes in proliferation and caspase activation in the Mcl-1 sensitive H929 cell line upon dosing with **42**. Proliferation data shown in red, caspase activation in black. (D) Viability studies on a panel of re-engineered BCR-ABL + B-ALL cells modified to have only the indicated antiapoptotic exogenous human Bcl-2 family member or deletion of Bax/Bak, DKO (double Bax, Bak knockout) treated with **42**.

from an Mcl-1 inhibitor. It was also demonstrated that **42** is selective for Mcl-1 and does not displace Bim from Bcl-xL (Figure 5B). Indeed, it appears that displacement of Bim from Mcl-1 by compound **42** causes a redistribution of Bim to Bcl-xL. The displacement of Bim from Mcl-1 is dose-dependent and correlates with the redistribution of Bim to Bcl-xL.

Another indicator of the on-target activity of **42** is that the dose-dependent decrease in proliferation observed in Mcl-1 sensitive cell lines is correlated with mechanism-based caspase activation. This is shown for **42** in Figure 5C, for the previously characterized Mcl-1 sensitive (H929) and insensitive (K562) cell lines. The sensitive cell line, H929, has growth inhibition and caspase activation at ~100 nM EC_{50}, whereas little growth inhibition is observed in the insensitive cell line K562, even at micromolar concentrations (data not shown). Compound **42** activity in proliferation experiments in a larger panel of heme cell lines is shown in Figure S2A, Supporting Information. In these experiments, compound **42** generally caused higher cytochrome *c* release in cell lines with lower GI_{50} in the proliferation assay (Figure S2B, Supporting Information). In addition, cytochrome *c* release caused by compound **42** is similar to that obtained from the Mcl-1 specific BH3 peptide MS-1 in these cell lines (Figure S2C, Supporting Information).[45]

To further test for specific on-target activity, compound **42** was tested in a panel of re-engineered BCR-ABL + B-ALL cells, that were modified to only contain a specific exogenous human Bcl-2 family protein (Figure 5D).[46−50] When these cell lines were dosed, a clear separation for the activity of compound **42** against cell lines with different Bcl-2 family proteins was observed. The cell line which only expressed human Mcl-1 as the antiapoptotic protein had the lowest EC_{50}. Compound **42** has 4−8-fold less activity against the Bcl-2- and Bcl-xL-engineered lines, respectively, with a minimal off-target toxicity even at high concentrations in the DKO (double Bax, Bak knockout) cell lines. The Mcl-1 specificity in the re-engineered cell lines is consistent with the results shown in the Co-IP experiments on the H929 cell line (Figure 5A,B) which demonstrates dose-dependent compound-mediated displacement of Bim from Mcl-1 and its redistribution to Bcl-xL.

Activity in Animal Tumor Models of Human Cancer. *Pharmacokinetic Profile of Compound 42.* After identifying compound **42** as a potent and selective Mcl-1 inhibitor in cellular assays, its suitability for progression into in vivo xenograft models was evaluated. Compound **42** was dosed at 3 mpk IV in rat and found to possess a reasonable clearance (CL = 38 mL/min/kg), Vd_{ss} (1.82), and exposure (1904 nM·h), providing significant improvements in clearance and exposure relative to the diazepinone congener. Dosing **42** via intraperitoneal (IP) administration in rat at 3 mpk showed that the compound possessed good permeability and was able to achieve a C_{max} of 626 nM and an AUC of 2041 nM·h. Exposure in mice (IP, 3 mpk) was somewhat lower with C_{max} = 272 nM and AUC = 523 nM·h. These results demonstrate that compound **42** can achieve an adequate exposure to test its efficacy in mouse xenograft models.

Hematologic Cancer Xenograft Models. Compound **42** was evaluated in growth inhibition assays with Mcl-1 sensitive cell lines AMO-1 (multiple myeloma) and MV-4-11 (acute leukemia) from which xenograft models had been generated. Compound **42** was found to be potent in heme cell lines, achieving a GI_{50} of 140 nM in AMO-1 and 70 nM in MV-4-11.

DOI: 10.1021/acs.jmedchem.8b01991
J. Med. Chem. 2019, 62, 3971−3988

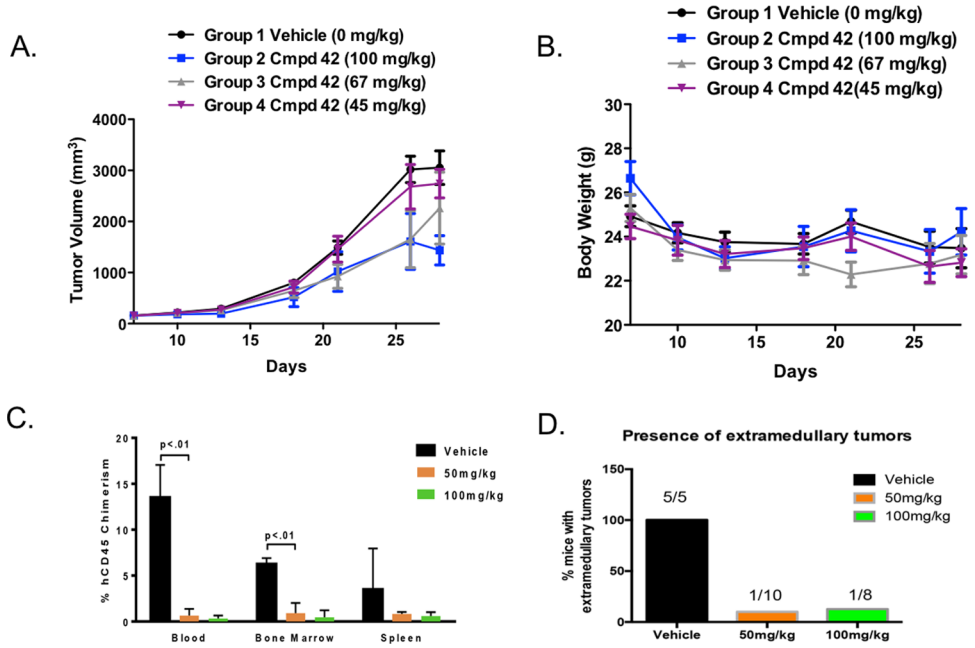

Figure 6. Efficacy of compound **42** in two different in vivo hematologic cancer models. (A) Tumor volume for AMO-1 tumor flank xenografts in immunocompromised mice. Dosed IP for 14 days at 100, 67, 45 mg/kg or vehicle. (B) Body weight for control and treatment groups in AMO-1 xenograft study. (C, D) MV-4-11 disseminated leukemia model. Dosing at 100, 50 mg/kg or vehicle IP for 21 days. (C) $CD45^+$ human leukemia chimerism at day 35. (D) Presence of extramedullary tumors in mice at day 35. Per arm vehicle (n = 5), 50 mg/kg (n = 10), and 100 mg/kg (n = 10). A nonparametric, unpaired, two-tailed t-test was used to calculate significance in (C).

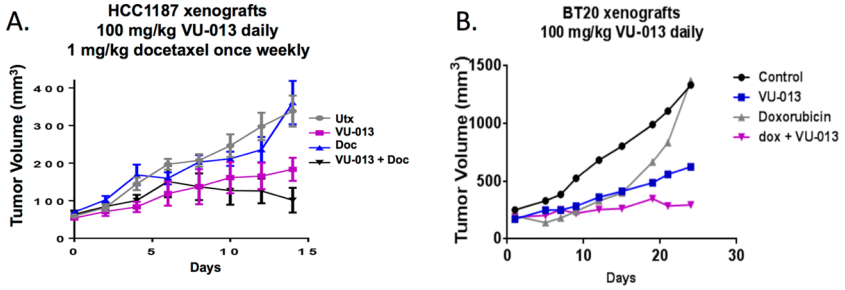

Figure 7. In vivo activity of **42**/VU-013 in human TNBC HCC-1187/BT-20 TNBC mouse tumor xenograft model. (A) HCC-1187 tumor size as a function of days with IP dosing of 100 mg/kg of **42**, DMSO vehicle control, docetaxol once weekly, or docetaxol + **42**. (B) BT-20 tumor size as a function of days (100 mg/kg of **42**, DMSO vehicle control, doxorubicin once weekly, or doxorubicin + **42**) with dosed IP.

Compound **42** was then tested in human multiple myeloma AMO-1 flank xenografts in immunocompromised mice. Tumors were grown to a volume of 200 mm^3 before starting daily IP dosing for 14 days. Growth inhibition was observed in a dose-dependent manner with the highest dose, 100 mg/kg, showing a 60% reduction in tumor growth compared to the DMSO vehicle (Figure 6A). Compound **42** was well tolerated over the 14 day dosing period showing no overt signs of toxicity or significant weight loss.

The in vivo activity of compound **42** was also evaluated in a secondary hemaotologic cancer model, based on the dissemination of a human acute myeloid leukemia (AML) cell line, MV-4-11, into immunodeficient mice. In this model, immunodeficient γ (NSG) mice were injected with MV-4-11 AML cells and monitored for tumor development.[44] MV-4-11 cell engraftment was confirmed by peripheral microchimerism 7 days post-transplant. Mice were then treated with the indicated doses of **42** for 3 weeks (days 14−35). At day 21 of treatment, vehicle mice became moribund, and all experimental mice were sacrificed for tissue analysis. Human cell tumor burden was determined by analyzing blood, bone marrow, and spleen samples for leukemia cells by CD45 flow cytometry. Vehicle-treated mice displayed florid leukemia, whereas almost no human CD45 leukemia cells could be detected in the blood of animals treated at the 50 or 100 mg/kg doses (Figure 6B). Human AML cells were also greatly reduced in bone marrow and spleen at these doses. Finally, dosing with **42** also prevented the formation of extramedullary tumors (Figure 6C). However, within 2 weeks of ending treatment with **42**, the mice become morbidly cytopenic and succumb to disseminated leukemia.

Triple Negative Breast Cancer (TNBC) Solid Tumor Animal Models. We evaluated the impact of compound **42** in xenograft models of human triple negative breast cancer (TNBC) using HCC-1187 and BT-20 cells. Interestingly, compound **42** exhibited a lower potency in TNBC cells (HCC-1187 GI_{50} = 1.3 μm, BT-20 GI_{50} = 2.1 μm) as compared to hematological cancer cells. Orthotopic HCC-1187 and BT-20 xenografts were generated in athymic Balb/C (nu/nu) mice. When tumors reached approximately 100 mm^3,

DOI: 10.1021/acs.jmedchem.8b01991
J. Med. Chem. 2019, 62, 3971−3988

Scheme 1. Representative Synthesis of Mcl-1 Inhibitors[a]

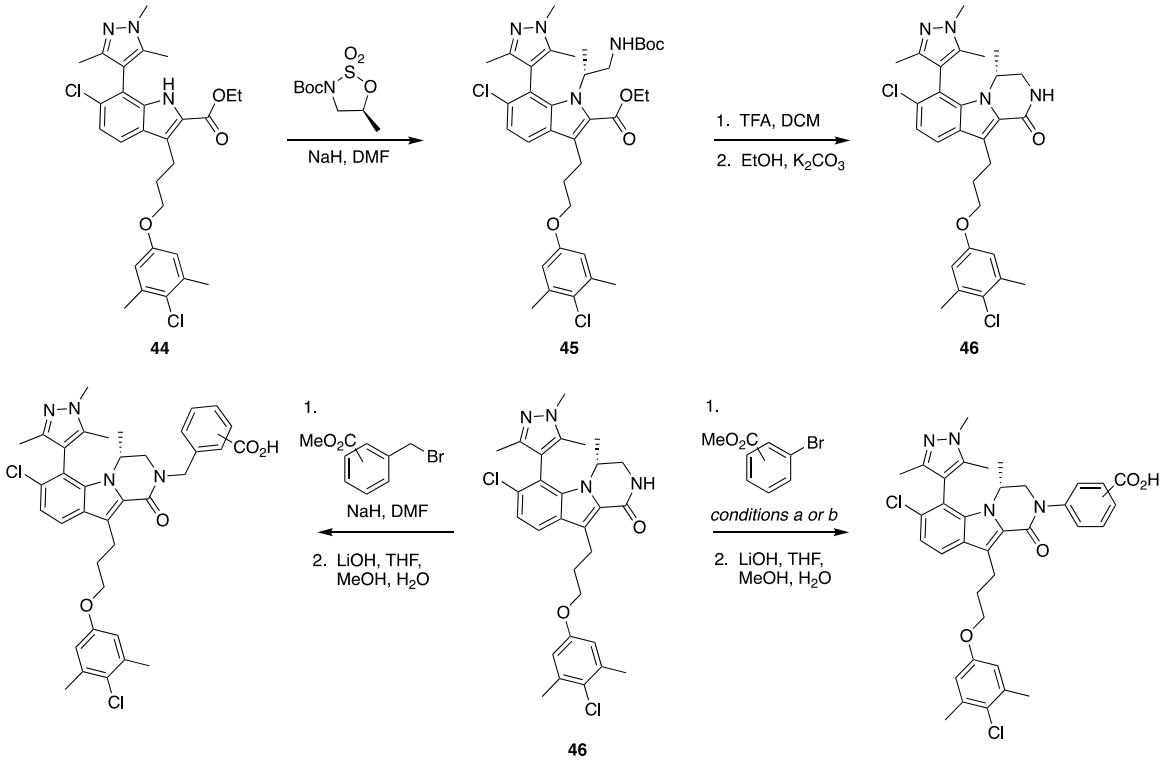

[a]Conditions: (a) CuI, *trans-N,N′*-dimethylaminocyclohexane, K_3PO_4, toluene, 110 °C; (b) Pd_2dba_3, Xantphos, Cs_2CO_3, dioxane, 110 °C.

mice were randomized to receive compound **42** (100 mg/kg) or vehicle for 14 days, monitoring weight and tumor volume daily. HCC-1187 tumors from mice treated with **42** displayed nearly 60% tumor growth inhibition (TGI) as compared to tumors treated with vehicle (Figure 7A). Similar results were seen in **42**-treated BT-20 tumors (Figure 7B). Immunohistochemical analysis revealed increased staining for cleaved caspase 3 in HCC-1187 and BT-20 tumors treated with **42** over vehicle-treated tumors (Figure S3A,B, Supporting Information), consistent with the induction of tumor cell apoptosis. At this dose, **42** was well tolerated by animals, as determined by daily weight monitoring (Figure S3C, Supporting Information).

Because TNBCs are treated with chemotherapy as the standard of care, we tested the impact of compound **42** on the response of HCC-1187 to the taxane docetaxel.[51] Although HCC-1187 cells were relatively resistant to docetaxel as a single agent, the combination of compound **42** with docetaxel resulted in tumor growth inhibition than either agent alone (Figure 7A), suggesting that **42** potently sensitizes HCC-1187 cells to docetaxel. Similarly, the growth of BT-20 xenografts treated with the combination of **42** and doxorubicin was inhibited to a greater extent than tumors treated with either agent alone (Figure 7B). When tested on HCC-1187/BT-20 cells in vitro, this combination was highly synergistic. As shown in Figure 7, even though the xenografts were relatively insensitive to once weekly docetaxel or doxorubicin dosing, the combination of docetaxel or doxorubicin plus **42** had a robust synergistic activity when compared to either agent alone.

Synthesis. The synthetic route employed for the indole core **44** has been previously reported. The methylated diazepinone and piperazinone tricyclic cores were synthesized by alkylation with the appropriate oxathiazinane or oxathiazolidine precursor, followed by *tert*-butoxycarbonyl (Boc) deprotection and cyclization under basic conditions to afford the desired tricyclic cores (Scheme 1). Elaboration to the final analogues (**2**–**43**) was accomplished by alkylation with the appropriate benzyl bromide or Ullmann coupling with the appropriate aryl bromide followed by saponification. The absolute configurations of *M*-**42** and *P*-**42** were determined by X-ray crystallography. Experimental details are described in the Supporting Information.

CONCLUSIONS

Improper regulation of Bcl-2 family members can increase the threshold for apoptosis in cancer cells allowing them to survive under conditions that normal cells would sense as aberrant and respond by inducing apoptosis. BH3 mimetics are a new class of drugs that target the antiapoptotic Bcl-2 family members to re-establish the sensitivity of cancer cells to stress. Mcl-1 inhibitors are potentially useful in a wide range of cancers, both as a single agent and in combination therapies. In this manuscript, we have described the design and synthesis of a potent and selective Mcl-1 inhibitor, **42**, which represents a chemically distinct class of Mcl-1 inhibitors that possess on-target activity in multiple cancer models. In addition to displaying cellular efficacy in multiple Mcl-1 sensitive cell lines, **42** presented a pharmacokinetics profile suitable for evaluation in mouse xenograft cancer models. We have shown that mouse tumor xenografts derived from Mcl-1 sensitive heme and breast cancer cell lines were also responsive to in vivo treatment, either as a single agent or in combination, with robust tumor regression being achieved in the MV-4-11 model of disseminated leukemia. The ability of this new class of Mcl-1 inhibitors to achieve regressions in tumor xenograft experi-

DOI: 10.1021/acs.jmedchem.8b01991
J. Med. Chem. 2019, 62, 3971−3988

ments compares favorably to Mcl-1 inhibitors that have recently entered phase I clinical trials. The novel chemotype and modular synthesis may provide opportunities to differentiate from extant classes of Mcl-1 inhibitors with regards to compound properties or tolerability. In comparison, the reported GI_{50} of S63845 is <10 nM in H929 cells,[38] demonstrating that significant further improvement in cellular efficacy by structural refinement is possible. Efforts are currently underway to continue exploring the therapeutic potential of the compound **42** as well as develop improved Mcl-1 inhibitors with compound dispositions suitable for the advancement to the clinic.

EXPERIMENTAL SECTION

Chemistry. *General.* All NMR spectra were recorded at room temperature (rt) on a 400 MHz AMX Bruker spectrometer. ^{1}H chemical shifts are reported in δ values in ppm downfield with the deuterated solvent as the internal standard. Data are reported as follows: chemical shift, multiplicity (s = singlet, d = doublet, t = triplet, q = quartet, br = broad, m = multiplet), integration, coupling constant (Hz). Low-resolution mass spectra (MS) were obtained on an Agilent 1200 series 6140 mass spectrometer with electrospray ionization (ESI). All samples were of ≥95% purity, as analyzed by liquid chromatography (LC)−UV/vis−MS. Analytical HPLC was performed on an Agilent 1200 series with UV detection at 214 and 254 nm along with ELSD detection. LC−MS parameters were as follows: method A: Phenomenex-C18 Kinetex column, 50 × 2.1 mm^2, 1 min gradient, 50% (0.1% trifluoroacetic acid (TFA)/MeCN)/50% (0.1% TFA/H_2O) to 100% (0.1% TFA/MeCN); method B: Phenomenex-C18 Kinetex column, 50 × 2.1 mm^2, 2 min gradient, 50% (0.1% TFA/MeCN)/50% (0.1% TFA/H_2O) to 95% (0.1% TFA/MeCN)/5% (0.1% TFA/H_2O); method C: Phenomenex-C18 Kinetex column, 50 × 2.1 mm^2, 2 min gradient, 5% (0.1% TFA/MeCN)/95% (0.1% TFA/H_2O) to 95% (0.1% TFA/MeCN)/95% (0.1% TFA/H_2O). Preparative purification was performed on a Gilson HPLC (Phenomenex-C18, 100 × 30 mm^2, 10 min gradient, 5 → 95% MeCN/H_2O with 0.1% TFA) or by automated flash column chromatography (ISCO, Inc. 100sg CombiFlash). Normal phase purification was performed with CombiFlash Rf (plus-UV) Automated Flash Chromatography System. Solvents for reactions, extraction, and washing were ACS reagent grade, and solvents for chromatography were HPLC grade. All reagents were purchased from chemical suppliers and used without purification. LC−MS traces for tested compounds are available in the Supporting Information (Section S6).

*General Procedures for the Synthesis of Diazepinone and Piperazinone Cores (**6, 7, 11, 15, 19, 23, 27, 31**). Indole Alkylation.* To a flame-dried round-bottom 50 mL flask equipped with a magnetic stir bar were added ethyl 6-chloro-3-(3-(4-chloro-3,5-dimethylphenoxy)propyl)-7-(4,6-dimethylpyrimidin-5-yl)-1*H*-indole-2-carboxylate (1.0 equiv), cesium carbonate (2.5 equiv), and anhydrous acetonitrile (20 mL). The corresponding sulfamate (2.5 equiv) was added, and the solution was stirred at 80 °C overnight. The reaction mixture was diluted with ethyl acetate (100 mL) and washed with brine (3 × 50 mL), dried with anhydrous $MgSO_4$, filtered, and then concentrated in vacuo. The residue was purified by flash column chromatography (CombiFlash Rf, EtOAc/hexane = 0−100% gradient) to afford the title compound.

Boc-Deprotection and Cyclization. The corresponding alkylated indole was dissolved in anhydrous dichloromethane (DCM) (20 mL) and cooled to 0 °C in an ice bath. Trifluoroacetic acid (8 equiv) was added dropwise, and the reaction mixture was allowed to stir at room temperature for 4 h. The solvent was removed using a rotary evaporator and dried under vacuum for 2 h. Anhydrous ethanol (20 mL) was added followed by anhydrous K_2CO_3 (15 equiv). The reaction mixture was stirred at 50 °C for 2 h. The reaction mixture was concentrated to 1/3 volume and diluted with ethyl acetate (100 mL) and washed with brine (3 × 50 mL). The combined organic layers were dried over anhydrous $MgSO_4$, filtered, and concentrated in vacuo. The residue was purified by flash column chromatography (CombiFlash Rf, DCM/methanol = 0−5% gradient) to afford the title compound.

*General Procedure for Alkylation of Diazepinone and Piperazinone Cores (**8−10, 12−14, 16−18, 20−22, 24−26, 28−30, 32−34**).* To a flame-dried round-bottom 25 mL flask equipped with a magnetic stir bar were added the corresponding lactam and anhydrous DMF (2 mL). The solution was stirred in an ice bath under a nitrogen atmosphere. Sodium hydride (60%) (2 equiv) was added and allowed to stir for 10 min. The corresponding alkyl halide (1.7 equiv) was then added, and the reaction was allowed to stir at 0 °C for 10 min and then at room temperature for 1 h. The reaction mixture was then diluted with ethyl acetate (20 mL) and washed with brine (2 × 10 mL), dried with anhydrous $MgSO_4$, filtered off, and concentrated down using rotary evaporator. The residue was dissolved in a mixture of tetrahydrofuran (THF) and MeOH (4 mL, 1:1), and NaOH (2 M, 1 mL) was added. The reaction was monitored by LC−MS for completion. The reaction mixture was neutralized with HCl (1 M), concentrated to half volume, diluted with ethyl acetate, and washed with water. The organic layer was concentrated down using a rotary evaporator and dissolved in a mixture of DMSO and MeOH and purified by HPLC (Phenomenex Gemini C18, H_2O/CH_3CN gradient from 50 to 95% CH_3CN for 4 min, 0.1% TFA) to afford the title compound.

*8-Chloro-11-(3-(4-chloro-3,5-dimethylphenoxy)propyl)-5-methyl-7-(1,3,5-trimethyl-1H-pyrazol-4-yl)-2,3,4,5-tetrahydro-1H-[1,4]-diazepino[1,2-a]indol-1-one (**6**).* Yield 20 mg, 6% for three steps; ^{1}H NMR ($CDCl_3$) δ 7.67 (d, J = 8 Hz, 1H), 7.26 (d, J = 8 Hz, 1H), 6.66 (s, 2H), 4.77−4.75 (m, 1H), 4.03 (tr, J = 8 Hz, 2H), 3.94 and 3.91 (two s, total 3H), 3.43−3.30 (m, 3H), 3.22−3.12 (m, 2H), 2.36 (s, 6H), 2.25−2.20 (m, 2H), 2.19 (s, 3H), 2.03 and 2.01 (two s, total 3H), 1.87−1.84 (m, 2H), 1.27 and 1.22 (two d, J = 8 Hz, total 3H). LC−MS method A: R_T = 0.89 min, MS (ESI): mass calcd for $C_{30}H_{34}Cl_2N_4O_2$, 552.2; m/z found, 553.2 $[M + H]^+$.

*8-Chloro-11-(3-(4-chloro-3,5-dimethylphenoxy)propyl)-4-methyl-7-(1,3,5-trimethyl-1H-pyrazol-4-yl)-2,3,4,5-tetrahydro-1H-[1,4]-diazepino[1,2-a]indol-1-one (**7**).* Yield 270 mg, 80% for three steps; ^{1}H NMR ($CDCl_3$) δ 7.62 (d, J = 8 Hz, 1H), 7.24 (d, J = 8 Hz, 1H), 6.65 (s, 2H), 5.97−5.95 (m, 1H), 4.06−4.03 (m, 1H), 3.97 (t, J = 8 Hz, 2H), 3.68 and 3.66 (two s, total 3H), 3.28−3.11 (m, 3H), 2.76−2.72 (m, 2H), 2.34 (s, 6H), 2.34 (tr, J = 8 Hz, 2H), 2.21 and 2.20 (two s, total 3H), 2.18 and 2.16 (two s, total 3H), 1.99 (m, 1H), 0.78 and 0.70 (two d, J = 8 Hz, total 3H). LC−MS method A: R_T = 0.91 min, MS (ESI): mass calcd for $C_{30}H_{34}Cl_2N_4O_2$, 552.2; m/z found, 553.2 $[M + H]^+$.

*3-((8-Chloro-11-(3-(4-chloro-3,5-dimethylphenoxy)propyl)-4-methyl-1-oxo-7-(1,3,5-trimethyl-1H-pyrazol-4-yl)-4,5-dihydro-1H-[1,4]diazepino[1,2-a]indol-2(3H)-yl)methyl)benzoic Acid (**8**).* Yield 27 mg, 73% for two steps; ^{1}H NMR ($CDCl_3$) δ 8.04 (d, J = 6 Hz, 1H), 8.02 (s, 1H), 7.64 (d, J = 8 Hz, 1H), 7.61 (m, 1H), 7.45 (tr, J = 6 Hz, 1H), 7.24 (d, J = 8 Hz, 1H), 6.64 (s, 2H), 5.10 (dd, J_1 = 16 Hz, J_2 = 28 Hz, 1H), 4.45 (dd, J_1 = 16 Hz, J_2 = 28 Hz, 1H), 4.05−4.01 (m, 3H), 3.89 and 3.88 (two s, total 3H), 3.79−3.72 (m, 4H), 3.27−3.24 (m, 1H), 3.22−3.11 (m, 2H), 2.28−2.82 (m, 1H), 2.82 (s, 6H), 2.33−2.24 (m, 2H), 2.22 and 2.20 (two s, total 3H), 2.09 and 1.98 (two s, total 3H), 1.90−1.80 (m, 1H), 0.59 and 0.53 (two d, J = 8 Hz, total 3H). LC−MS method A: R_T = 0.95 min, MS (ESI): mass calcd for $C_{38}H_{40}Cl_2N_4O_4$, 686.2; m/z found, 687.2 $[M + H]^+$.

*4-((8-Chloro-11-(3-(4-chloro-3,5-dimethylphenoxy)propyl)-4-methyl-1-oxo-7-(1,3,5-trimethyl-1H-pyrazol-4-yl)-4,5-dihydro-1H-[1,4]diazepino[1,2-a]indol-2(3H)-yl)methyl)benzoic Acid (**9**).* Yield 30 mg, 82% for two steps; LC−MS method A: R_T = 0.94 min, MS (ESI): mass calcd for $C_{38}H_{40}Cl_2N_4O_4$, 686.2; m/z found, 687.2 $[M + H]^+$.

*5-((8-Chloro-11-(3-(4-chloro-3,5-dimethylphenoxy)propyl)-4-methyl-1-oxo-7-(1,3,5-trimethyl-1H-pyrazol-4-yl)-4,5-dihydro-1H-[1,4]diazepino[1,2-a]indol-2(3H)-yl)methyl)furan-2-carboxylic Acid (**10**).* Yield 33 mg, 92% for two steps; LC−MS method A: R_T = 0.91 min, MS (ESI): mass calcd for $C_{36}H_{38}Cl_2N_4O_5$, 676.2; m/z found, 677.2 $[M + H]^+$.

DOI: 10.1021/acs.jmedchem.8b01991
J. Med. Chem. 2019, 62, 3971−3988

*8-Chloro-11-(3-(4-chloro-3,5-dimethylphenoxy)propyl)-3-methyl-7-(1,3,5-trimethyl-1H-pyrazol-4-yl)-2,3,4,5-tetrahydro-1H-[1,4]-diazepino[1,2-a]indol-1-one (**11**).* Yield 200 mg, 64% for three steps; ^{1}H NMR ($CDCl_3$) δ 7.61 (d, J = 8 Hz, 1H), 7.22 (d, J = 8 Hz, 1H), 6.65 (s, 2H), 5.51−5.32 (m, 1H), 4.25−4.15 (m, 1H), 4.10−3.95 (m, 2H), 3.70 and 3.68 (two s, total 3H), 3.80−3.70 (m, 1H), 3.50−3.45 (m, 1H), 3.35−3.30 (m, 1H), 3.15−3.05 (m, 1H), 2.34 (s, 6H), 2.25−2.20 (m, 1H), 2.05 (s, 3H), 2.04 (two s, total 3H), 1.88−1.86 (m, 1H), 1.49−1.44 (m, 1H), 1.16 (d, J = 8 Hz, 3H). LC−MS method A: R_T = 0.86 min, MS (ESI): mass calcd for $C_{30}H_{34}Cl_2N_4O_2$, 552.2; m/z found, 553.6 $[M + H]^+$.

*3-((8-Chloro-11-(3-(4-chloro-3,5-dimethylphenoxy)propyl)-3-methyl-1-oxo-7-(1,3,5-trimethyl-1H-pyrazol-4-yl)-4,5-dihydro-1H-[1,4]diazepino[1,2-a]indol-2(3H)-yl)methyl)benzoic Acid (**12**).* Yield 15 mg, 50% for two steps; ^{1}H NMR ($CDCl_3$) δ 8.05 (d, J = 6 Hz, 1H), 8.00 (s, 1H), 7.66 (m, 1H), 7.64 (d, J = 8 Hz, 1H), 7.43 (tr, J = 6 Hz, 1H), 7.22 (d, J = 8 Hz, 1H), 6.66 (s, 2H), 5.03 (dd, J_1= 16 Hz, J_2 = 28 Hz, 1H), 4.60 (dd, J_1 = 16 Hz, J_2 = 28 Hz, 1H), 4.05−3.98 (m, 3H), 3.89 (s, 3H), 3.65−3.60 (m, 2H), 3.33−3.25 (m, 1H), 3.19−3.10 (m, 1H), 2.33 (s, 6H), 2.33−2.24 (m, 2H), 2.05 and 2.03 (two s, total 3H), 2.09 and 1.98 (two s, total 3H), 1.88−1.86 (m, 2H), 1.08 and 1.03 (two d, J = 8 Hz, 3H). LC−MS method A: R_T = 0.89 min, MS (ESI): mass calcd for $C_{38}H_{40}Cl_2N_4O_4$, 686.2; m/z found, 687.1 $[M + H]^+$.

*4-((8-Chloro-11-(3-(4-chloro-3,5-dimethylphenoxy)propyl)-3-methyl-1-oxo-7-(1,3,5-trimethyl-1H-pyrazol-4-yl)-4,5-dihydro-1H-[1,4]diazepino[1,2-a]indol-2(3H)-yl)methyl)benzoic Acid (**13**).* Yield 16 mg, 52% for two steps; LC−MS method A: R_T = 0.88 min, MS (ESI): mass calcd for $C_{38}H_{40}Cl_2N_4O_4$, 686.2; m/z found, 687.1 $[M + H]^+$.

*5-((8-Chloro-11-(3-(4-chloro-3,5-dimethylphenoxy)propyl)-3-methyl-1-oxo-7-(1,3,5-trimethyl-1H-pyrazol-4-yl)-4,5-dihydro-1H-[1,4]diazepino[1,2-a]indol-2(3H)-yl)methyl)furan-2-carboxylic Acid (**14**).* Yield 15 mg, 49% for two steps; LC−MS method A: R_T = 0.85 min, MS (ESI): mass calcd for $C_{36}H_{38}Cl_2N_4O_5$, 676.2; m/z found, 677.2 $[M + H]^+$.

*7-Chloro-10-(3-(4-chloro-3,5-dimethylphenoxy)propyl)-6-(1,3,5-trimethyl-1H-pyrazol-4-yl)-3,4-dihydropyrazino[1,2-a]indol-1(2H)-one (**15**).* Yield 400 mg, 81% for three steps; ^{1}H NMR ($CDCl_3$) δ 7.65 (d, J = 8 Hz, 1H), 7.26 (d, J = 8 Hz, 1H), 6.65 (s, 2H), 5.96 (broad s, 1H), 4.03 (tr, J = 8 Hz, 2H), 3.85 (s, 3H), 3.81−3.79 (m, 1H), 3.73−3.68 (m, 1H), 3.54−3.48 (m, 2H), 3.39 (tr, J = 8 Hz, 2H), 2.37 (s, 6H), 2.19 (tr, J = 8 Hz, 2H), 2.12 (s, 3H), 2.05 (s, 3H). LC−MS method A: R_T = 0.85 min, MS (ESI): mass calcd for $C_{28}H_{30}Cl_2N_4O_2$, 524.1; m/z found, 525.2 $[M + H]^+$.

*3-((7-Chloro-10-(3-(4-chloro-3,5-dimethylphenoxy)propyl)-1-oxo-6-(1,3,5-trimethyl-1H-pyrazol-4-yl)-3,4-dihydropyrazino[1,2-a]indol-2(1H)-yl)methyl)benzoic Acid (**16**).* Yield 22 mg, 73% for two steps; ^{1}H NMR ($CDCl_3$) δ 8.04 (d, J = 8 Hz, 1H), 8.01 (s, 1H), 7.67 (d, J = 8 Hz, 1H), 7.61 (d, 4 Hz, 1H), 7.45 (tr, J = 8 Hz, 1H), 7.26 (d, J = 8 Hz, 1H), 6.67 (s, 2H), 4.87 (q, J_1 = 16 Hz, J_2 = 36 Hz, 2H), 4.75 (tr, J = 8 Hz, 2H), 3.89 (s, 3H), 3.76−3.72 (m, 1H), 3.65−3.61 (m, 1H), 3.50−3.39 (m, 4H), 2.35 (s, 6H), 2.25 (tr, J = 8 Hz, 2H), 2.06 (s, 3H), 2.05 (s, 3H). LC−MS method A: R_T = 0.95 min, MS (ESI): mass calcd for $C_{36}H_{36}Cl_2N_4O_4$, 658.2; m/z found, 659.2 $[M + H]^+$.

*4-((7-Chloro-10-(3-(4-chloro-3,5-dimethylphenoxy)propyl)-1-oxo-6-(1,3,5-trimethyl-1H-pyrazol-4-yl)-3,4-dihydropyrazino[1,2-a]indol-2(1H)-yl)methyl)benzoic Acid (**17**).* Yield 20 mg, 66% for two steps; LC−MS method A: R_T = 0.93 min, MS (ESI): mass calcd for $C_{36}H_{36}Cl_2N_4O_4$, 658.2; m/z found, 659.2 $[M + H]^+$.

*5-((7-Chloro-10-(3-(4-chloro-3,5-dimethylphenoxy)propyl)-1-oxo-6-(1,3,5-trimethyl-1H-pyrazol-4-yl)-3,4-dihydropyrazino[1,2-a]indol-2(1H)-yl)methyl)furan-2-carboxylic Acid (**18**).* Yield 18 mg, 60% for two steps; LC−MS method A: R_T = 0.89 min, MS (ESI): mass calcd for $C_{34}H_{34}Cl_2N_4O_5$, 648.2; m/z found, 649.2 $[M + H]^+$.

*(S)-7-Chloro-10-(3-(4-chloro-3,5-dimethylphenoxy)propyl)-4-methyl-6-(1,3,5-trimethyl-1H-pyrazol-4-yl)-3,4-dihydropyrazino-[1,2-a]indol-1(2H)-one (**19**).* Yield 450 mg, 77% for three steps; ^{1}H NMR ($CDCl_3$) δ 7.67 (d, J = 8 Hz, 1H), 7.26 (d, J = 8 Hz, 1H), 6.65 (s, 2H), 5.65−5.64 (m, 1H), 4.24−4.21 (m, 1H), 4.14−4.11 (m, 1H), 4.04−4.01 (m, 2H), 3.89 (s, 3H), 3.83−3.70 (m, 1H), 3.46−3.43 (m, 1H), 3.41−3.37 (m, 1H), 3.25−3.20 (m, 1H), 2.37 (s, 6H), 2.29 (m, 2H), 2.24 and 2.22 (two s, total 3H), 2.24 and 2.19 (two s, total 3H), 1.16 and 0.98 (two d, J = 8 Hz, total 3H). LC−MS method A: R_T = 0.88, 0.90 min, MS (ESI): mass calcd for $C_{29}H_{32}Cl_2N_4O_2$, 538.2; m/z found, 539.4 $[M + H]^+$.

*(S)-3-((7-Chloro-10-(3-(4-chloro-3,5-dimethylphenoxy)propyl)-4-methyl-1-oxo-6-(1,3,5-trimethyl-1H-pyrazol-4-yl)-3,4-dihydropyrazino[1,2-a]indol-2(1H)-yl)methyl)benzoic Acid (**20**).* Yield 25 mg, 89% for two steps; ^{1}H NMR ($CDCl_3$) δ 8.06 (d, J = 8 Hz, 1H), 8.05 (s, 1H), 7.68 (d, J = 8 Hz, 1H), 7.63 (d, 1H, 4 Hz), 7.46 (t, J = 8 Hz, 1H), 7.26 (d, J = 8 Hz, 1H), 6.67 (s, 2H), 5.17 (dd, J_1 = 16 Hz, J_2 = 28 Hz, 1H), 4.64 (dd, J_1 = 16 Hz, J_2 = 28 Hz, 1H), 3.80 (m, 3H), 3.96 (s, 3H), 3.76−3.72 (m, 1H), 3.67−3.41 (m, 2H), 3.20−3.16 (m, 1H), 2.25 (s, 6H), 2.17 (tr, J = 8 Hz, 2H), 2.15 and 2.13 (two s, total 3H), 2.08 and 2.06 (two s, total 3H), 0.75 and 0.68 (two d, total J = 8 Hz, 3H). LC−MS method A: R_T = 0.85 min, MS (ESI): mass calcd for $C_{37}H_{38}Cl_2N_4O_4$, 672.2; m/z found, 673.1 $[M + H]^+$.

*(S)-4-((7-Chloro-10-(3-(4-chloro-3,5-dimethylphenoxy)propyl)-4-methyl-1-oxo-6-(1,3,5-trimethyl-1H-pyrazol-4-yl)-3,4-dihydropyrazino[1,2-a]indol-2(1H)-yl)methyl)benzoic Acid (**21**).* Yield 25 mg, 78% for two steps; LC−MS method A: R_T = 0.95 min, MS (ESI): mass calcd for $C_{37}H_{38}Cl_2N_4O_4$, 672.2; m/z found, 673.0 $[M + H]^+$.

*(S)-5-((7-Chloro-10-(3-(4-chloro-3,5-dimethylphenoxy)propyl)-4-methyl-1-oxo-6-(1,3,5-trimethyl-1H-pyrazol-4-yl)-3,4-dihydropyrazino[1,2-a]indol-2(1H)-yl)methyl)furan-2-carboxylic Acid (**22**).* Yield 15 mg, 54% for two steps; LC−MS method A: R_T = 0.90 min, MS (ESI): mass calcd for $C_{35}H_{36}Cl_2N_4O_5$, 662.2; m/z found, 663.0 $[M + H]^+$.

*(R)-7-Chloro-10-(3-(4-chloro-3,5-dimethylphenoxy)propyl)-4-methyl-6-(1,3,5-trimethyl-1H-pyrazol-4-yl)-3,4-dihydropyrazino-[1,2-a]indol-1(2H)-one (**23**).* Yield 280 mg, 75% for three steps; ^{1}H NMR ($CDCl_3$) δ 7.67 (d, J = 8 Hz, 1H), 7.26 (d, J = 8 Hz, 1H), 6.65 (s, 2H), 5.65−5.64 (m, 1H), 4.24−4.21 (m, 1H), 4.14−4.11 (m, 1H), 4.04−4.01 (m, 2H), 3.89 (s, 3H), 3.83−3.70 (m, 1H), 3.46−3.43 (m, 1H), 3.41−3.37 (m, 1H), 3.25−3.20 (m, 1H), 2.37 (s, 6H), 2.29 (m, 2H), 2.22 (s, 3H), 1.98 (s, 3H), 1.05 and 0.98 (two d, J = 8 Hz, total 3H). LC−MS method A: R_T = 0.84, 0.86 min, MS (ESI): mass calcd for $C_{29}H_{32}Cl_2N_4O_2$, 538.2; m/z found, 539.6 $[M + H]^+$.

*(R)-3-((7-Chloro-10-(3-(4-chloro-3,5-dimethylphenoxy)propyl)-4-methyl-1-oxo-6-(1,3,5-trimethyl-1H-pyrazol-4-yl)-3,4-dihydropyrazino[1,2-a]indol-2(1H)-yl)methyl)benzoic Acid (**24**).* Yield 18 mg, 72% for two steps; ^{1}H NMR ($CDCl_3$) δ 8.03 (d, J = 8 Hz, 1H), 8.01 (s, 1H), 7.66 (d, J = 8 Hz, 1H), 7.64 (d, 4 Hz, 1H), 7.46 (tr, J = 8 Hz, 1H), 7.26 (d, J = 8 Hz, 1H), 6.67 (s, 2H), 5.17 (dd, J_1 = 16 Hz, J_2 = 28 Hz, 1H), 4.64 (dd, J_1 = 16 Hz, J_2 = 28 Hz, 1H), 4.07−4.05 (m, 3H), 3.92 (s, 3H), 3.76−3.72 (m, 1H), 3.51−3.36 (m, 2H), 3.12−3.09 (m, 1H), 2.35 (s, 6H), 2.24 (tr, J = 8 Hz, 2H), 2.18 and 2.16 (two s, total 3H), 2.01 and 1.98 (two s, total 3H), 0.85 and 0.77 (two d, J = 8 Hz, total 3H). LC−MS method A: R_T = 0.79 min, MS (ESI): mass calcd for $C_{37}H_{38}Cl_2N_4O_4$, 672.2; m/z found, 673.0 $[M + H]^+$.

*(R)-4-((7-Chloro-10-(3-(4-chloro-3,5-dimethylphenoxy)propyl)-4-methyl-1-oxo-6-(1,3,5-trimethyl-1H-pyrazol-4-yl)-3,4-dihydropyrazino[1,2-a]indol-2(1H)-yl)methyl)benzoic Acid (**25**).* Yield 12 mg, 48% for two steps; LC−MS method A: R_T = 0.88 min, MS (ESI): mass calcd for $C_{37}H_{38}Cl_2N_4O_4$, 672.2; m/z found, 673.0 $[M + H]^+$.

*(R)-5-((7-Chloro-10-(3-(4-chloro-3,5-dimethylphenoxy)propyl)-4-methyl-1-oxo-6-(1,3,5-trimethyl-1H-pyrazol-4-yl)-3,4-dihydropyrazino[1,2-a]indol-2(1H)-yl)methyl)furan-2-carboxylic Acid (**26**).* Yield 8 mg, 32% for two steps; LC−MS method A: R_T = 0.73 min, MS (ESI): mass calcd for $C_{35}H_{36}Cl_2N_4O_5$, 662.2; m/z found, 663.0 $[M + H]^+$.

*(R)-7-Chloro-10-(3-(4-chloro-3,5-dimethylphenoxy)propyl)-3-methyl-6-(1,3,5-trimethyl-1H-pyrazol-4-yl)-3,4-dihydropyrazino-[1,2-a]indol-1(2H)-one (**27**).* Yield 237 mg, 82% for three steps; ^{1}H NMR ($CDCl_3$) δ 7.65 (d, J = 8 Hz, 1H), 7.26 (d, J = 8 Hz, 1H), 6.65 (s, 2H), 5.72 (m, 1H), 4.02 (tr, J = 8 Hz, 2H), 3.82 (s, 3H), 3.78−3.73 (m, 2H), 3.38−3.30 (m, 3H), 2.35 (s, 6H), 2.23 (tr, J = 8 Hz, 2H), 2.06 (s, 3H), 2.04 (s, 3H), 1.21 and 1.18 (two d, J = 4 Hz, total

DOI: 10.1021/acs.jmedchem.8b01991
J. Med. Chem. 2019, 62, 3971−3988

3H). LC−MS method A: R_T = 0.95 min, MS (ESI): mass calcd for $C_{29}H_{32}Cl_2N_4O_2$, 538.2; m/z found, 539.1 $[M + H]^+$.

*(R)-3-((7-Chloro-10-(3-(4-chloro-3,5-dimethylphenoxy)propyl)-3-methyl-1-oxo-6-(1,3,5-trimethyl-1H-pyrazol-4-yl)-3,4-dihydropyrazino[1,2-a]indol-2(1H)-yl)methyl)benzoic Acid (**28**).* Yield 26 mg, 68% for two steps; ^{1}H NMR ($CDCl_3$) δ 8.04 (d, J = 8 Hz, 1H), 8.00 (s, 1H), 7.68 (d, J = 8 Hz, 1H), 7.65 (d, 4 Hz, 1H), 7.46 (tr, J = 8 Hz, 1H), 7.26 (d, J = 8 Hz, 1H), 6.67 (s, 2H), 5.58 (dd, J_1= 8 Hz, J_2 = 12 Hz, 1H), 5.52 (dd, J_1 = 16 Hz, J_2 = 28 Hz, 1H), 4.04−4.00 (m, 3H), 3.87 and 3.69 (two s, total 3H), 3.60−3.55 (m, 3H), 3.45−3.37 (m, 2H), 2.35 (s, 6H), 2.24 (tr, J = 8 Hz, 2H), 2.08−2.04 (several s, total 6H), 1.14 and 0.57 (two d, J = 8 Hz, total 3H). LC−MS method A: R_T = 1.01 min, MS (ESI): mass calcd for $C_{37}H_{38}Cl_2N_4O_4$, 672.2; m/z found, 673.2 $[M + H]^+$.

*(R)-4-((7-Chloro-10-(3-(4-chloro-3,5-dimethylphenoxy)propyl)-3-methyl-1-oxo-6-(1,3,5-trimethyl-1H-pyrazol-4-yl)-3,4-dihydropyrazino[1,2-a]indol-2(1H)-yl)methyl)benzoic Acid (**29**).* Yield 31 mg, 81% for two steps; LC−MS method A: R_T = 1.01 min, MS (ESI): mass calcd for $C_{37}H_{38}Cl_2N_4O_4$, 672.2; m/z found, 673.2 $[M + H]^+$.

*(R)-5-((7-Chloro-10-(3-(4-chloro-3,5-dimethylphenoxy)propyl)-3-methyl-1-oxo-6-(1,3,5-trimethyl-1H-pyrazol-4-yl)-3,4-dihydropyrazino[1,2-a]indol-2(1H)-yl)methyl)furan-2-carboxylic Acid (**30**).* Yield 28 mg, 67% for two steps; LC−MS method A: R_T = 0.96 min, MS (ESI): mass calcd for $C_{35}H_{36}Cl_2N_4O_5$, 662.2; m/z found, 663.2 $[M + H]^+$.

*(S)-7-Chloro-10-(3-(4-chloro-3,5-dimethylphenoxy)propyl)-3-methyl-6-(1,3,5-trimethyl-1H-pyrazol-4-yl)-3,4-dihydropyrazino-[1,2-a]indol-1(2H)-one (**31**).* Yield 170 mg, 90% for three steps; ^{1}H NMR ($CDCl_3$) δ 7.64 (d, J = 8 Hz, 1H), 7.26 (d, J = 8 Hz, 1H), 6.65 (s, 2H), 5.73 (m, 1H), 4.03 (tr, J = 8 Hz, 2H), 3.82 (s, 3H), 3.78−3.73 (m, 2H), 3.38−3.30 (m, 3H), 2.35 (s, 6H), 2.21 (tr, J = 8 Hz, 2H), 2.07 (s, 3H), 2.04 (s, 3H), 1.21 and 1.19 (two d, J = 4 Hz, total 3H). LC−MS method A: R_T = 0.90 min, MS (ESI): mass calcd for $C_{29}H_{32}Cl_2N_4O_2$, 538.2; m/z found, 539.2 $[M + H]^+$.

*(S)-3-((7-Chloro-10-(3-(4-chloro-3,5-dimethylphenoxy)propyl)-3-methyl-1-oxo-6-(1,3,5-trimethyl-1H-pyrazol-4-yl)-3,4-dihydropyrazino[1,2-a]indol-2(1H)-yl)methyl)benzoic Acid (**32**).* Yield 29 mg, 92% for two steps; ^{1}H NMR ($CDCl_3$) δ 8.00 (d, J = 8 Hz, 1H), 7.98 (s, 1H), 7.67 (d, J = 8 Hz, 1H), 7.60 (d, 4 Hz, 1H), 7.45 (tr, J = 8 Hz, 1H), 7.26 (d, J = 8 Hz, 1H), 6.67 (s, 2H), 5.59 (dd, J_1 = 8 Hz, J_2 = 12 Hz, 1H), 5.54 (dd, J_1 = 16 Hz, J_2 = 28 Hz, 1H), 4.04−3.90 (m, 3H), 3.86 and 3.68 (two s, total 3H), 3.60−3.55 (m, 3H), 3.47−3.35 (m, 2H), 2.35 (s, 6H), 2.24 (m, 2H), 2.05 (s, 3H), 2.03 (s, 3H), 1.11 and 1.07 (two d, J = 8 Hz, total 3H). LC−MS method A: R_T = 1.00 min, MS (ESI): mass calcd for $C_{37}H_{38}Cl_2N_4O_4$, 672.2; m/z found, 673.2 $[M + H]^+$.

*(S)-4-((7-Chloro-10-(3-(4-chloro-3,5-dimethylphenoxy)propyl)-3-methyl-1-oxo-6-(1,3,5-trimethyl-1H-pyrazol-4-yl)-3,4-dihydropyrazino[1,2-a]indol-2(1H)-yl)methyl)benzoic Acid (**33**).* Yield 25 mg, 80% for two steps; LC−MS method A: R_T = 1.00 min, MS (ESI): mass calcd for $C_{37}H_{38}Cl_2N_4O_4$, 672.2; m/z found, 673.2 $[M + H]^+$.

*(S)-5-((7-Chloro-10-(3-(4-chloro-3,5-dimethylphenoxy)propyl)-3-methyl-1-oxo-6-(1,3,5-trimethyl-1H-pyrazol-4-yl)-3,4-dihydropyrazino[1,2-a]indol-2(1H)-yl)methyl)furan-2-carboxylic Acid (**34**).* Yield 25 mg, 81% for two steps; LC−MS method A: R_T = 0.93 min, MS (ESI): mass calcd for $C_{35}H_{36}Cl_2N_4O_5$, 662.2; m/z found, 663.2 $[M + H]^+$.

General Procedure A: Ullmann Cross-Coupling. To a flame-dried 2 dram equipped with a magnetic stir bar were added (*R*)-7-chloro-10-(3-(4-chloro-3,5-dimethylphenoxy)propyl)-4-methyl-6-(1,3,5-trimethyl-1*H*-pyrazol-4-yl)-3,4-dihydropyrazino[1,2-*a*]indol-1(2*H*)-one (1 equiv), methyl 3-bromo-1-methyl-1*H*-indole-5-carboxylate (2 equiv), CuI (0.2 equiv), and K_3PO_4 (3 equiv). *trans*-*N*,*N*′-Dimethylcyclohexane-1,2-diamine (0.2 equiv) in toluene (1 mL) was added, and the reaction was sparged with argon for 5 min. The reaction was then sealed and heated to 110 °C for 48−72 h. The reaction was then diluted with DCM/H_2O (10 mL, 1:1). The organic layer was separated, and the aqueous layer was extracted with DCM (2 × 5 mL). The combined organic fractions were combined, dried with a phase separator, and concentrated in vacuo. The residue was purified by flash column chromatography, eluting with 0−100% EtOAc/hexane. The ester was then dissolved in THF/MeOH/H_2O (2/0.5/0.5 mL), and LiOH (5 equiv) was added. The reaction was heated to 40 °C until complete by LC−MS. The reaction was then concentrated in vacuo, dissolved in MeOH/DMSO (1 mL), and purified by reverse phase HPLC (Phenomenex Gemini C18, H_2O/CH_3CN gradient from 50 to 95% CH_3CN for 4 min, 0.1% TFA) to afford the title compound.

*(R)-3-(7-Chloro-10-(3-(4-chloro-3,5-dimethylphenoxy)propyl)-4-methyl-1-oxo-6-(1,3,5-trimethyl-1H-pyrazol-4-yl)-3,4-dihydropyrazino[1,2-a]indol-2(1H)-yl)benzoic Acid (**35**).* The title compound was prepared following General Procedure A. Yield 16 mg, 53% for two steps; ^{1}H NMR ($CDCl_3$) δ 8.02 (d, J = 8 Hz, 1H), 8.00 (s, 1H), 7.72 (d, J = 8 Hz, 1H), 7.69 (d, 4 Hz, 1H), 7.56 (t, J = 8 Hz, 1H), 7.32 (d, J = 8 Hz, 1H), 6.65 (s, 2H), 4.44−4.00 (m, 1H), 4.01 (tr, J = 8 Hz, 2H), 3.96 (s, 3H), 3.46−3.37 (m, 1H), 3.35−3.32 (m, 1H), 2.33 (s, 6H), 2.25 (m, 4H), 2.19 and 2.17 (two s, total 3H), 2.09 and 2.07 (two s, total 3H), 1.18 and 1.11 (two d, J = 6 Hz, total 3H). LC−MS method A: R_T = 0.98 min, MS (ESI): mass calcd for $C_{36}H_{36}Cl_2N_4O_4$, 658.2; m/z found, 659.6 $[M + H]^+$.

*(R)-4-(7-Chloro-10-(3-(4-chloro-3,5-dimethylphenoxy)propyl)-4-methyl-1-oxo-6-(1,3,5-trimethyl-1H-pyrazol-4-yl)-3,4-dihydropyrazino[1,2-a]indol-2(1H)-yl)benzoic Acid (**36**).* The title compound was prepared following General Procedure A. Yield 22 mg, 68% for two steps; ^{1}H NMR ($CDCl_3$) δ 8.10 (d, J = 4 Hz, 2H), 7.66 (d, J = 8 Hz, 1H), 7.40 (d, J = 8 Hz, 2H), 7.26 (d, J = 8 Hz, 1H), 6.57 (s, 2H), 4.39−4.37 (m, 1H), 4.02−4.00 (m, 5H), 3.47−3.42 (m, 1H), 3.37−3.32 (m, 1H), 2.34 (s, 6H), 2.28 and 2.25 (two s, total 3H), 2.22 (tr, J = 8 Hz, 2H), 2.18 (m, 2H), 2.12 and 2.10 (two s, total 3H), 1.15 and 1.10 (two d, J = 6 Hz, total 3H). LC−MS method B R_T = 2.23 min, MS (ESI): mass calcd for $C_{36}H_{36}Cl_2N_4O_4$, 658.2; m/z found, 658.9 $[M + H]^+$.

*(R)-6-(7-Chloro-10-(3-(4-chloro-3,5-dimethylphenoxy)propyl)-4-methyl-1-oxo-6-(1,3,5-trimethyl-1H-pyrazol-4-yl)-3,4-dihydropyrazino[1,2-a]indol-2(1H)-yl)-1-methyl-1H-indole-4-carboxylic Acid (**37**).* The title compound was prepared following General Procedure A. Yield 41 mg, 62% for two steps. ^{1}H NMR (400 MHz, DMSO-d_6) δ 7.74−7.73 (m, 3H), 7.51 (d, J = 1.6 Hz, 1H), 7.28 (d, J = 6.8 Hz, 1H), 6.92 (d, J = 2.4 Hz, 1H), 6.72 (s, 2H), 4.53 (d, J = 8.0 Hz, 1H), 4.16−4.12 (m, 1H), 3.97−3.94 (m, 2H), 3.82 (s, 3H), 3.77 (s, 3H), 3.69 (dd, J = 18.4, 10.8 Hz, 1H), 3.33−3.16 (m, 2H), 2.23 (s, 6H), 2.11 (s, 1.5H), 2.06−2.03 (m, 2H), 2.02 (s, 1.5H), 1.97 (s, 1.5H), 1.87 (s, 1.5H), 1.04 (d, J = 8.4 Hz, 3H). LC−MS method A R_T = 0.89 min, MS (ESI): mass calcd for $C_{39}H_{39}Cl_2N_5O_4$, 711.2; m/z found, 712.0 $[M + H]^+$.

*(R)-4-(7-Chloro-10-(3-(4-chloro-3,5-dimethylphenoxy)propyl)-4-methyl-1-oxo-6-(1,3,5-trimethyl-1H-pyrazol-4-yl)-3,4-dihydropyrazino[1,2-a]indol-2(1H)-yl)-1-methyl-1H-indole-6-carboxylic Acid (**38**).* To a flame-dried round-bottom 25 mL flask equipped with a magnetic stir bar were added 7-chloro-10-(3-(4-chloro-3,5-dimethylphenoxy)propyl)-4-methyl-6-(1,3,5-trimethyl-1*H*-pyrazol-4-yl)-3,4-dihydropyrazino[1,2-*a*]indol-1(2*H*)-one and anhydrous 1,4-dioxane (2 mL). Sequentially, Cs_2CO_3 (1.8 equiv), $Pd_2(dba)_3$ (2 mol %), xanthpos (7 mol %), and the corresponding aryl bromide (1.2 equiv) were added. The reaction mixture was stirred at 120 °C overnight. The reaction was worked up, saponified, and purified following procedure described in General Procedure A. Yield 15 mg, 65% for two steps. ^{1}H NMR ($CDCl_3$) δ 8.16 (s, 1H), 7.76 (d, J = 8 Hz, 1H), 7.73 (s, 1H), 7.26 (d, J = 8 Hz, 1H), 7.24 (d, J = 8 Hz, 1H), 6.57 (s, 2H), 6.40 (d, J = 8 Hz, 1H), 4.55−4.50 (m, 1H), 4.21 (m, 2H), 3.99 (s, 3H), 3.91 (s, 3H), 3.69−3.65 (m, 1H), 3.46−3.37 (m, 2H), 2.32 (s, 6H), 2.29 and 2.26 (two s, total 3H), 2.29 (t, J = 8 Hz, 2H), 2.18 (m, 2H), 2.13 and 2.11 (two s, total 3H), 1.27 and 1.20 (two d, J = 6 Hz, total 3H). LC−MS method A: R_T = 0.76 min, MS (ESI): mass calcd for $C_{39}H_{39}Cl_2N_5O_4$, 711.2; m/z found, 712.0 $[M + H]^+$.

*(R)-7-(7-Chloro-10-(3-(4-chloro-3,5-dimethylphenoxy)propyl)-4-methyl-1-oxo-6-(1,3,5-trimethyl-1H-pyrazol-4-yl)-3,4-dihydropyrazino[1,2-a]indol-2(1H)-yl)benzo[d][1,3]dioxole-5-carboxylic Acid (**39**).* **Methyl 7-Iodobenzo[*d*][1,3]dioxole-5-carbox-**

DOI: 10.1021/acs.jmedchem.8b01991
J. Med. Chem. 2019, 62, 3971−3988

ylate: In a vial equipped with a stir bar, 7-bromobenzo[*d*][1,3]-dioxole-5-carboxylic acid (250 mg, 1.02 mmol) was dissolved in THF (3.4 mL) and methanol (0.6 mL). $TMSCHN_2$ (0.77 mL, 1.53 mmol, 2.0 M in diethyl ether) was added and stirred at rt for 10 min. The reaction was quenched with 0.6 mL of glacial acetic acid, and the reaction was concentrated in vacuo. The resulting white solid (~250 mg) was redissolved in 1,4-dioxane (1 mL). (1*R*,2*R*)-N^1,N^2-Dimethylcyclohexane-1,2-diamine (16 μL, 0.1 mmol, *d* = 0.9 g/mL), copper iodide (19 mg, 0.1 mmol), and sodium iodide (450 mg, 3 mmol) were added to the reaction mixture. The reaction vial was purged with argon for 5 min and heated at 110 °C for 24 h. The reaction was quenched with 30% aqueous NH_4OH and extracted with DCM (3 × 15 mL). The combined organic layers were washed with brine and dried over $MgSO_4$ and concentrated in vacuo. The resultant crude reaction mixture was then purified by silica gel chromatography using a Teledyne ISCO CombiFlash and eluting with 10−100% EtOAc in hexane to afford the title compound (290 mg, 93% yield, two steps). LC−MS: R_T = 1.586 min, MS (ESI) 306.9 (M + H).

(*R*)-7-(7-Chloro-10-(3-(4-chloro-3,5-dimethylphenoxy)propyl)-4-methyl-1-oxo-6-(1,3,5-trimethyl-1*H*-pyrazol-4-yl)-3,4-dihydropyrazino[1,2-*a*]indol-2(1*H*)-*yl*)benzo[*d*][1,3]dioxole-5-carboxylic Acid (39): The title compound was prepared (75 mg, 77% yield over two steps) following General Procedure A using (*R*)-7-chloro-10-(3-(4-chloro-3,5-dimethylphenoxy)propyl)-4-methyl-6-(1,3,5-trimethyl-1*H*-pyrazol-4-yl)-3,4-dihydropyrazino[1,2-*a*]indol-1(2*H*)-one (75 mg, 0.139 mmol) and methyl 7-iodobenzo[*d*][1,3]-dioxole-5-carboxylate (106 mg, 0.35 mmol). ^{1}H NMR (400 MHz, DMSO-d_6) δ 7.75 (d, *J* = 8.6 Hz, 1H), 7.59−7.57 (m, 1H), 7.34 (d, *J* = 1.4 Hz, 1H), 7.29 (d, *J* = 8.6 Hz, 1H), 6.74 (s, 2H), 6.18 (s, 1H), 6.16 (d, *J* = 2.1 Hz, 1H), 4.39 (dt, *J* = 12.9, 3.7 Hz, 1H), 4.19−4.08 (m, 1H), 4.03−3.93 (m, 2H), 3.78 (s, 1.5H), 3.77 (s, 1.5H), 3.63 (dd, *J* = 18.5, 11.9 Hz, 1H), 3.33−3.26 (m, 1H), 3.25−3.18 (m, 1H), 2.26 (s, 6H), 2.10 (s, 1.5H), 2.09−2.02 (m, 2H), 2.01 (s, 1.5H), 1.95 (s, 1.5H), 1.86 (s, 1.5H), 1.03−0.96 (m, 3H). LC−MS method A: R_T = 0.83 min, MS (ESI): mass calcd for $C_{37}H_{36}Cl_2N_4O_6$, 702.2; *m*/*z* found, 703.0 $[M + H]^+$.

*5-(7-Chloro-10-(3-(4-chloro-3,5-dimethylphenoxy)propyl)-4-methyl-1-oxo-6-(1,3,5-trimethyl-1H-pyrazol-4-yl)-3,4-dihydropyrazino[1,2-a]indol-2(1H)-yl)-1-naphthoic Acid (**40**).* The title compound was prepared (86 mg, 0.12 mmol, 32% yield over two steps) as a white solid following General Procedure A using 5-bromo-1-naphthoic acid (250 mg, 1.0 mmol). ^{1}H NMR (400 MHz, DMSO-d_6): 8.87 (dd, *J* = 13.8, 8.7 Hz, 1H), 8.16 (t, *J* = 7.2 Hz, 1H), 8.09−8.04 (m, 1H), 7.78 (d, *J* = 8.6 Hz, 1H), 7.72−7.68 (m, 1H), 7.64−7.49 (m, 2H), 7.32−7.29 (m 1H), 6.69−6.68 (m, 2H), 4.68−4.58 (m, 1H), 4.24−4.18 (m, 1H), 4.05−3.94 (m, 3H), 3.78−3.74 (m, 3H), 3.61−3.53 (m, 1H), 3.25−3.18 (m, 1H), 2.23 (s, 6H), 2.13−1.98 (m, 8H), 1.91−1.90 (m, 1H), 1.19−1.15 (m, 3H); >98% at 215 nm. LC−MS method B: R_T = 2.27 min, MS (ESI) calcd for $C_{40}H_{38}Cl_2N_4O_4$, 708.2; *m*/*z* found, 708.9 $(M + H)^+$.

*(R)-3-(7-Chloro-10-(3-(4-chloro-3,5-dimethylphenoxy)propyl)-4-methyl-1-oxo-6-(1,3,5-trimethyl-1H-pyrazol-4-yl)-3,4-dihydropyrazino[1,2-a]indol-2(1H)-yl)-1-methyl-1H-indole-6-carboxylic Acid (**41**).* The title compound (30 mg, 84% yield over two steps) was prepared following General Procedure A using (*R*)-7-chloro-10-(3-(4-chloro-3,5-dimethylphenoxy)propyl)-4-methyl-6-(1,3,5-trimethyl-1*H*-pyrazol-4-yl)-3,4-dihydropyrazino[1,2-*a*]indol-1(2*H*)-one (27 mg, 0.05 mmol) and methyl 3-bromo-1-methyl-1*H*-indole-6-carboxylate (16 mg, 0.06 mmol). ^{1}H NMR (400 MHz, DMSO-d_6) δ 8.17 (s, 1H), 7.76 (d, *J* = 8.5 Hz, 1H), 7.67 (d, *J* = 3.0 Hz, 1H), 7.66−7.62 (m, 1H), 7.48 (dd, *J* = 8.5, 4.4 Hz, 1H), 7.30 (d, *J* = 8.5 Hz, 1H), 6.72 (s, 2H), 4.48 (dd, *J* = 13.2, 4.0 Hz, 1H), 4.18−4.14 (m, 1H), 4.02−3.96 (m, 2H), 3.88 (s, 3H), 3.79 (d, *J* = 3.8 Hz, 3H), 3.66 (t, *J* = 11.6 Hz, 1H), 3.36−3.19 (m, 2H), 2.55 (s, 6H), 2.12 (s, 2H), 2.10−2.05 (m, 2H), 2.03 (s, 1H), 1.98 (s, 1H), 1.89 (s, 2H), 1.08 (d, *J* = 6.4 Hz, 3H). LC−MS method B: R_T = 1.32 min, MS (ES): mass calcd for $C_{39}H_{39}Cl_2N_5O_4$, 711.2; *m*/*z* found, 711.9 $(M + H)^+$.

*(R)-3-(7-Chloro-10-(3-(4-chloro-3,5-dimethylphenoxy)propyl)-4-methyl-1-oxo-6-(1,3,5-trimethyl-1H-pyrazol-4-yl)-3,4-dihydropyrazino[1,2-a]indol-2(1H)-yl)-1-methyl-1H-indole-5-carboxylic Acid (**42**).* The title compound (28 mg, 79% yield over two steps) was prepared following General Procedure A using (*R*)-7-chloro-10-(3-(4-chloro-3,5-dimethylphenoxy)propyl)-4-methyl-6-(1,3,5-trimethyl-1*H*-pyrazol-4-yl)-3,4-dihydropyrazino[1,2-*a*]indol-1(2*H*)-one (27 mg, 0.05 mmol) and methyl 3-bromo-1-methyl-1*H*-indole-5-carboxylate (16 mg, 0.06 mmol). ^{1}H NMR (400 MHz, DMSO-d_6) δ 8.11 (dd, *J* = 3.5, 1.5 Hz, 1H), 7.87−7.71 (m, 2H), 7.57 (dd, *J* = 9.4, 1.9 Hz, 2H), 7.30 (d, *J* = 8.6 Hz, 1H), 6.73 (s, 2H), 4.48 (dd, *J* = 13.0, 3.8 Hz, 1H), 4.24−4.09 (m, 1H), 3.99 (tt, *J* = 6.4, 3.2 Hz, 2H), 3.85 (s, 3H), 3.79 (s, 1.5H), 3.77 (s, 1.5H), 3.72−3.59 (m, 1H), 3.23 (dt, *J* = 13.4, 7.4 Hz, 2H), 2.24 (s, 6H), 2.12 (s, 1.5H), 2.07 (dd, *J* = 12.7, 6.0 Hz, 2H), 2.03 (s, 1.5H), 1.98 (s, 1.5H), 1.89 (s, 1.5H), 1.19−0.93 (m, 3H). LC−MS method C: R_T = 1.96 min, MS (ES): mass calcd for $C_{39}H_{39}Cl_2N_5O_4$, 711.2; *m*/*z* found, 712.0 $(M + H)^+$.

*Separation of Atropisomers of **23**.* The mixture of atropisomers of tricyclic piperazinone **23** was dissolved in DMSO and purified by reverse phase HPLC (Phenomenex Gemini C18, H_2O/CH_3CN gradient from 50 to 95% CH_3CN for 10 min, 0.1% TFA) to afford ~40% of each atropisomer. Once separated, the atropisomers showed no interconversion after 72 h at 100 °C in DMSO. The absolute stereochemistry was confirmed by X-ray crystallography. (*M*)-(*R*)-7-Chloro-10-(3-(4-chloro-3,5-dimethylphenoxy)propyl)-4-methyl-6-(1,3,5-trimethyl-1*H*-pyrazol-4-yl)-3,4-dihydropyrazino[1,2-*a*]indol-1(2*H*)-one (second eluting atropisomer), LC−MS method B: R_T = 1.25 min, ^{1}H NMR (400 MHz, $CDCl_3$): 7.65 (d, *J* = 8.6 Hz, 1H), 7.26 (d, *J* = 8.6 Hz, 1H), 6.65 (s, 2H), 6.02 (d, *J* = 5.0 Hz, 1H), 4.23 (quint, *J* = 5.2 Hz, 1H), 4.06−3.97 (m, 2H), 3.88 (s, 3H), 3.83 (dd, *J* = 12.6, 4.0 Hz, 1H), 3.46−3.30 (m, 2H), 3.21 (ddd, *J* = 7.2, 5.4, 1.2 Hz), 2.34 (s, 6H), 2.24−2.19 (m, 2H), 2.18 (s, 3H), 1.99 (s, 3H), 0.98 (d, *J* = 6.3 Hz, 3H). (*P*)-(*R*)-7-Chloro-10-(3-(4-chloro-3,5-dimethylphenoxy)propyl)-4-methyl-6-(1,3,5-trimethyl-1*H*-pyrazol-4-yl)-3,4-dihydropyrazino[1,2-*a*]indol-1(2*H*)-one (first eluting atropisomer), LC−MS method B: R_T = 1.12 min, ^{1}H NMR (400 MHz, $CDCl_3$): 7.56 (d, *J* = 8.4 Hz, 1H), 7.18 (d, *J* = 8.4 Hz, 1H), 6.55 (s, 2H), 6.01 (d, *J* = 5.0 Hz, 1H), 4.05 (quint, *J* = 5.2 Hz, 1H), 3.96−3.88 (m, 2H), 3.78 (s, 3H), 3.71 (dd, *J* = 12.4, 3.9 Hz, 1H), 3.37−3.20 (m, 2H), 3.12 (ddd, *J* = 12.3, 5.2, 1.1 Hz, 1H), 2.25 (s, 6H), 2.15−2.10 (m, 2H), 2.08 (s, 3H), 1.89 (s, 3H), 0.95 (d, *J* = 6.5 Hz, 3H).

*(M)-(R)-3-(7-Chloro-10-(3-(4-chloro-3,5-dimethylphenoxy)-propyl)-4-methyl-1-oxo-6-(1,3,5-trimethyl-1H-pyrazol-4-yl)-3,4-dihydropyrazino[1,2-a]indol-2(1H)-yl)-1-methyl-1H-indole-5-carboxylic Acid ((M)-**42**).* The title compound was prepared analogously to compound **42** using (*M*)-(*R*)-7-chloro-10-(3-(4-chloro-3,5-dimethylphenoxy)propyl)-4-methyl-6-(1,3,5-trimethyl-1*H*-pyrazol-4-yl)-3,4-dihydropyrazino[1,2-*a*]indol-1(2*H*)-one. ^{1}H NMR (400 MHz, DMSO-d_6): 8.10 (s, 1H), 7.82 (d, *J* = 8.8 Hz, 1H), 7.75 (d, *J* = 8.6 Hz, 1H), 7.52−7.45 (m, 2H), 7.29 (d, *J* = 8.5 Hz, 1H), 6.73 (s, 2H), 4.47 (dd, *J* = 10.0, 3.6 Hz, 1H), 4.21−4.16 (m, 1H), 4.02−3.88 (m, 2H), 3.83 (s, 3H), 3.77 (s, 3H), 3.66 (d, *J* = 12.5 Hz, 1H), 3.36−3.21 (m, 2H), 2.24 (s, 6H), 2.11 (s, 3H), 2.07−2.04 (m, 2H), 1.89 (s, 3H), 1.09 (d, *J* = 6.3 Hz, 3H). LC−MS method C: R_T = 2.15 min, MS (ESI): mass calcd for $C_{39}H_{39}Cl_2N_5O_4$, 711.2; *m*/*z* found, 711.9 $(M + H)^+$.

*(P)-(R)-3-(7-Chloro-10-(3-(4-chloro-3,5-dimethylphenoxy)-propyl)-4-methyl-1-oxo-6-(1,3,5-trimethyl-1H-pyrazol-4-yl)-3,4-dihydropyrazino[1,2-a]indol-2(1H)-yl)-1-methyl-1H-indole-5-carboxylic Acid ((P)-**42**).* The title compound was prepared analogously to compound **42** using (*P*)-(*R*)-7-chloro-10-(3-(4-chloro-3,5-dimethylphenoxy)propyl)-4-methyl-6-(1,3,5-trimethyl-1*H*-pyrazol-4-yl)-3,4-dihydropyrazino[1,2-*a*]indol-1(2*H*)-one. ^{1}H NMR (400 MHz, DMSO-d_6): 8.12 (d, *J* = 1.1 Hz, 1H), 7.81 (dd, *J* = 8.7, 1.5 Hz, 1H), 7.76 (d, *J* = 8.6 Hz, 1H), 7.58−7.56 (m, 2H), 7.30 (d, *J* = 8.6 Hz, 1H), 6.73 (s, 2H), 4.48 (dd, *J* = 13.0, 3.7 Hz, 1H), 4.16−4.14 (m, 1H), 4.01−3.96 (m, 2H), 3.85 (s, 3H), 3.77 (s, 3H), 3.66 (d, *J* = 11.8 Hz, 1H), 3.36−3.21 (m, 2H), 2.24 (s, 6H), 2.07 (d, *J* = 6.6 Hz, 2H), 2.03 (s, 3H), 1.98 (s, 3H), 1.09 (d, *J* = 6.5 Hz, 3H). LC−MS method C: R_T = 2.13 min, MS (ESI): mass calcd for $C_{39}H_{39}Cl_2N_5O_4$, 711.2; *m*/*z* found, 711.9 $(M + H)^+$.

DOI: 10.1021/acs.jmedchem.8b01991
J. Med. Chem. 2019, 62, 3971−3988

*(S)-3-(7-Chloro-10-(3-(4-chloro-3,5-dimethylphenoxy)propyl)-4-methyl-1-oxo-6-(1,3,5-trimethyl-1H-pyrazol-4-yl)-3,4-dihydropyrazino[1,2-a]indol-2(1H)-yl)-1-methyl-1H-indole-5-carboxylic Acid (**43**).* The title compound (16 mg, 70% yield over two steps) was prepared analogously to compound **42** starting with (*S*)-7-chloro-10-(3-(4-chloro-3,5-dimethylphenoxy)propyl)-4-methyl-6-(1,3,5-trimethyl-1*H*-pyrazol-4-yl)-3,4-dihydropyrazino[1,2-*a*]indol-1(2*H*)-one. ^{1}H NMR (MeOH-d_4) δ 8.25 (d, J = 1.6 Hz, 1H), 7.95 (d, J = 8 Hz, 1H), 7.75 (dd, J_1 = 12 Hz, J_2 = 4 Hz, 1H), 7.51 (d, J = 8 Hz, 1H), 7.38 (d, J = 4 Hz, 1H), 7.29 (d, J = 12 Hz, 1H), 6.53 (s, 2H), 4.46 (dt, J_1 = 16 Hz, J_2 = 4 Hz, 1H), 4.30−4.28 (m, 1H), 4.05−3.94 (m, 2H), 3.89 (s, 3H), 3.87 (s, 3H), 3.73 (d, J = 8 Hz, 0.5H), 3.70 (d, J = 8 Hz, 0.5H), 3.52−3.41 (m, 1H), 3.34−3.33 (m, 1H), 2.31 (s, 6H), 2.26 (s, 1.5H), 2.20 (m, 2H), 2.17 (s, 1.5H), 2.08 (s, 1.5H), 2.00 (s, 1.5H), 1.23 and 1.21 (two overplaying d, J = 8 Hz, total 3H). MS (ESI): mass calcd for $C_{39}H_{39}Cl_2N_5O_4$, 711.2; m/z found, 712.2 $[M + H]^+$.

Protein Expression and Purification for Assays and X-ray Structures. Protein preparation was described previously.[40] Briefly, a previously reported construct was subcloned into an expression vector (pDEST-HisMBP) expressed in *Escherichia coli* BL21 CodonPlus (DE3) RIL (Stratagene) and purified through nickel-column and size-exclusion chromatography sequentially.

Protein Crystallization, Data Collection, and Structure Refinement. Structural studies were performed, as previously described.[39−43] Briefly, Mcl-1 protein (15 mg/mL) was mixed with a 1.2× excess of ligand in solution (25−30% poly(ethylene glycol) (PEG) 3350, 0.1 M Bis−Tris pH 6.5, 0.2 M $MgCl_2$) by hanging drop followed by flash freezing after cryo-protection using 10−20% glycol. Data were collected at Life Sciences Collaborative Access Team (LS-CAT) 21-ID-G beamline, Advanced Photon Source (APS), Argonne National Laboratory. Indexing, integration, and scaling were performed with HKL2000 (HKL Research),[52] phasing by molecular replacement with Phaser (CCP4)[53,54] using the structure (PDB: 4HW2) as a model, refinement used Phenix.[55,56] Structural statistics are given in the Supporting Information. Figures were prepared with PyMOL (Schrödinger, LLC, New York, 2010).

Competition Binding Assays. A fluorescein isothiocyanate (FITC)-labeled BH3 peptide derived from Bim (FITC-Bim; FITC-AHx-EARIAQELRRIGDEFNETYTR-NH2) or Bak (FITC-Bak; FITC-AHx-GQVGRQLAIIGDDINR-NH2) was purchased from Genscript and used without further purification. FPA measurements were made using 384-well, black, flat-bottom plates (Greiner Bio-One) and a BioTek Cytation 3.

FITC-Bim Assay Conditions. 20 mM Tris pH 7.5, 50 mM NaCl, 3 mM dithiothreitol (DTT), 0.01% 3-[(3-cholamidopropyl)-dimethylammonio]-1- propanesulfonate, FITC-Bim peptide at 1 nM and His6-MBP Mcl-1 at 1.5 nM.

Bcl-xL and Bcl-2 Assay Conditions. FITC-Bak peptide (10 nM) incubated with either 15 nM Mcl-1, 4 nM Bcl-xL, or 4 nM Bcl-2 in 20 mM Tris pH 7.5, 50 mM NaCl, 3 mM DTT, and 5% final DMSO. Fetal calf serum (1%) is added in 1% FBS assay. For IC_{50} determination, compounds were diluted in DMSO (10-point, threefold serial dilutions), added to assay plates, and incubated for 0.5 h at room temperature. The change in anisotropy was measured and used to calculate an IC_{50} (inhibitor concentration at which 50% of bound probe is displaced) by fitting the anisotropy data using XLFit (IDBS) to a four-parameter dose−response (variable slope) equation. This was converted to a binding dissociation constant (K_i) according to the formula: [56] $K_i = [I]_{50}/([L]_{50}/K_d + [P]_0/K_d + 1)$, where $[I]_{50}$ is the concentration of the free inhibitor at 50% inhibition, $[L]_{50}$ is the concentration of the free protein at 0% inhibition, and K_d^{pep} represents the dissociation constant of the FITC-labeled peptide probe. Compounds were evaluated using replicate measurements in duplicate; K_i values shown are the average of duplicate values.

TR-FRET Assay Conditions. FITC-labeled BAK peptide (300 nM), 1 nM Mcl-1-MBP fusion, 1 nM MBP-terbium (Cisbio, Bedford, MA), and compound were incubated in a buffer containing 4.5 mM monobasic potassium phosphate, 15.5 mM dibasic potassium phosphate, 1 mM ethylenediaminetetraacetic acid, 50 mM NaCl, 1 mM DTT, 0.05% Pluronic F-68, pH 7.5. Mixtures were incubated for 3 h, and signal (ΔF) was measured on the Biotek Cytation 3 equipped with a filter cube containing an Ex 340/30 nM Em 620/10 filter and an Ex 340/30 Em 520 filter. IC_{50} values were calculated by fitting anisotropy using XLFit (IDBS) and converted into a binding dissociation constant using the Cheng−Prusoff equation to generate a K_i. Two or more repeats were obtained, and average K_i values are reported.

Generation of Engineered Cell Lines. As described previously,[44] human BCL-xL, BCL-w, BCL-2 and BFL-1 cDNAs, and a BCR-ABL (p185) oncofusion plasmid were stably expressed in Mcl-1 conditional Arf-deficient bone marrow by retroviral transduction and puromycin selection. Endogenous murine Mcl-1 was deleted by transduction with Cre recombinase. For dosing experiments, engineered cell lines were seeded in 96-well round-bottom plates. Mcl-1 inhibitors were solubilized in DMSO, or DMSO vehicle controls were added at the indicated concentrations, and cells were in complete Roswell Park Memorial Institute (RPMI) media with 1% FBS. After 24 h, the plates were centrifuged, and cell viability was determined by staining with Annexin-V-APC and propidium iodide (BD Biosciences, San Jose, CA) and measured by flow cytometry using the high-throughput sampler on a FACSCanto II (BD Biosciences).

Cell Line Proliferation Assay. AMO-1 and HCC-1187 were maintained in RPMI, H929 cells were maintained in the RPMI supplemented with 0.05 mM β mercaptoethanol. MV-4-11 and K562 cell lines were maintained in Iscove's modified Dulbecco medium. The cell line BT-20 was propagated in Eagle's minimum essential medium. All cell culture media were supplemented with 10% FBS. For proliferation assays, 3000 cells were dispensed in 96-well plates. Suspension cells were plated immediately before the compound addition. Adherent cell lines were incubated overnight at 37 °C in a tissue culture incubator prior to compound addition. Dose responses were generated in DMSO and added to the cells. The final DMSO concentration was 0.5%. Plates were incubated for 72 h, and cell viability was measured using the CellTiter-Glo reagent (Promega, Madison, WI). %Viability was defined as relative luminescence units (RLU) of each well divided by the RLU of cells on day 0. Dose−response curves were generated, and GI_{50} values were determined using the XLFit (IDBS) software.

Caspase Activation Assay. Cells were dispensed in 96-well plates as described in the proliferation assay methods with 5% FBS and a cell concentration of 5000 cells per well in a 100 μL volume. Plates are incubated with the compound for 3 h, 50 μL of Caspase-Glo (Promega, Madison, WI) reagent is added, and the mixture was incubated at room temperature in the dark for 30 min. Luminescence was measured (Biotek Cytation 3) and analyzed using XLFit (IDBS) to generate EC_{50} values.

Energy Minimization of Conformations Using Maestro. The tricyclic core was drawn with the appropriate stereochemistry using the Maestro Ligand 2D Workspace. The structure was energy minimized with Macromodel (Maestro) using standard parameters (Forcefield: OPLS3, Mini: PRCG). All structures were superimposed to each other and to crystal structures using the SMARTS Keys of the constant portions of the core (NC(=O)ccc1cc(c)c(Cl)cc1). The superimposed structures were exported to Pymol for visualization.

Co-IP Experiment Mcl-1/Bim, Bcl-xL/Bim, Bcl-2/Bim in NCI-H929 Cell Line. NCI-H929 (10 million) cells were treated with compound at 31.25, 62.5, 125, 250, 500, and 1000 nM for 90 min. An additional sample was treated with 0.1% DMSO alone as a vehicle control. Cells were pelleted, washed in phosphate-buffered saline (PBS), and lysed in nondenaturing lysis buffer (50 mM Tris (pH 7.4), 150 mM NaCl, 2.5 mM $MgCl_2$ 0.5% NP40, protease/phosphatase inhibitor), and 800 μg of total cell lysate in a 400 μL volume was incubated with 4 μg of biotin-conjugated anti-Mcl-1 clone RC-13 (MA5-13929, Thermo Fisher scientific), 4 μg of biotin-conjugated anti-Bcl-xL clone 7B2.5 (AB25062, Abcam), or biotin-conjugated mouse IgG1 Isotype control (PA-5-33199, Thermo Fisher Scientific), followed by the addition of 30 μL of washed Dynabeads M-280 Streptavidin (11205D, Thermo Fisher Scientific). Beads were washed followed by the addition of LI-

DOI: 10.1021/acs.jmedchem.8b01991
J. Med. Chem. 2019, 62, 3971−3988

COR protein loading buffer (LI-COR, 928-40004) diluted in RIPA buffer at 95 °C. Bim and Mcl-1 were measured by western blot using rabbit anti-Bim clone Y36 (AB32158, Abcam), polyclonal anti-Mcl-1 (SC-819, Santa Cruz Biotechnology), monoclonal anti-rabbit Bcl-2 clone, and monoclonal anti-rabbit Bcl-xL Clone 54H6 (Cell Signaling Technologies, #2764) followed by IRDye secondary antibodies. Blots were scanned and image analysis performed on a LI-COR Odyssey.

Xenograft Flank Tumor Model with AMO-1. Female SCID mice (6−10 week old) were used for transplantation with human the multiple myeloma human cell line AMO-1. Mice were inoculated with 1×10^6 AMO-1 tumor cells subcutaneously into the flank of animal. The tumor cells were resuspended in matrigel (BD Biosciences). The width and length of the tumors were measured daily using an electronic caliper. When the tumor volume reached approximately 200 mm^3, mice were randomized into treatment and control groups ($n = 8$) with **42** (different concentrations) or vehicle. The compound was diluted in DMSO and administrated by intraperitoneal (IP) injection daily at the doses described in the figure legends. Mice were weighed, and tumor volume was measured daily. Tumor volume was calculated as: volume = length × $width^2$ × 0.52. Tumor growth inhibition (TGI_{max}) was calculated using: TGI_{max} (%) = (1 − (median of treated at day x − median of treated at day 0)/(median of control at day x − median of control at day 0) × 100) where x is the day maximum where the number of animals per group in the control group is sufficient to calculate TGI (%). For the statistical analysis of differences in tumor volume between treatment groups, a two-way analysis of variance with repeated measures on day factor was performed on log-transformed data.

In Vivo Tumor Model with MV-4-11. Female NSGS mice (NOD/SCID/Tg(hSCF/hGM-CSF/hIL3, 6−8 weeks old)) were sublethally irradiated (1 Gy) the day before intravenous injection with MV-4-11 cells (1×10^6). Engraftment was confirmed by the peripheral microchimerism of $hCD45^+$ cells at 7 days post-transplant. After confirmation of chimerism, mice were randomly divided into three groups and treated with vehicle or **42** at 100, or 50 mg/kg body weight, daily by IP for 3 weeks. Compound **42** was diluted in DMSO and administered via IP injection, with vehicle mice receiving DMSO. At the end of dosing, all mice were sacrificed, and tumor burden was determined by analyzing blood, bone marrow, and spleen samples for leukemia burden by CD45 flow cytometry. For flow cytometric analysis of chimerism, red blood cells were lysed with EL buffer on ice (Qiagen), with remaining cells washed and resupsended in 1× PBS with 1% bovine serum albumin and stained for 15 min with the following antibodies: human CD45-APC (BioLegend), human CD33-PE-Cy7 (BioLegend), murine CD45-PE (BioLegend) and DAPI (BioLegend). Cells were washed and submitted for flow cytometric analysis using a three-laser LSRII (Becton Dickinson).

Xenograft Flank Tumor Model with HCC-1187. All animals were conducted in accordance to guidelines approved by the IACUC at Vanderbilt University Medical Center. HCC-1187 cells were purchased in 2012 from ATCC and cultured at low passage in Dulbecco's modified Eagle's medium with 10% fetal calf serum and 1% antimycotic antibiotic reagent (Gibco). Cell identity was verified by ATCC using genotyping with a Multiplex STR assay. Cells were screened monthly for mycoplasma. All cell lines were used for experiments within 50 passages from thawing. For generation of orthotopic breast cancer xenografts, 1×10^6 HCC-1187 cells were injected into the inguinal mammary fatpads of athymic Balb/C nu/nu female mice (4−6 weeks old, Jax Mice). Tumor dimensions were measured using digital calipers. Tumor volume was calculated as: volume = length × $width^2$ × 0.52. When tumors reached 50−100 mm^3, mice were randomized into treatment groups to receive daily treatment with 100 mg/kg **42** in 50% poly(ethylene glycol)-400, 2.5% DMSO in sterile saline by intraperitoneal injection or equal volume of vehicle control, in combination with docetaxel (1 mg/kg) or vehicle (sterile saline) once weekly by intraperitoneal injection. Mice were weighed twice weekly.

Xenograft Flank Tumor Model with BT-20. All animals were conducted in accordance to guidelines approved by the IACUC at Vanderbilt University Medical Center. For generation of orthotopic breast cancer xenografts, 1×10^6 BT-20 cells were injected into the inguinal mammary fatpads of athymic Balb/C nu/nu female mice (4−6 weeks old, Jax Mice). Tumor dimensions were measured using digital calipers. Tumor volume was calculated as: volume = length × $width^2$ × 0.52. When tumors reached 50−100 mm^3, mice were randomized into treatment groups to receive daily treatment with 100 mg/kg **42** in 50% poly(ethylene glycol)-400, 2.5% DMSO in sterile saline by intraperitoneal injection or equal volume of vehicle control, in combination with doxorubicin (2 mg/kg) or vehicle (sterile saline) once weekly by intraperitoneal injection. Mice were weighed twice weekly.

■ ASSOCIATED CONTENT

Supporting Information

The Supporting Information is available free of charge on the ACS Publications website at DOI: 10.1021/acs.jmedchem.8b01991.

X-ray data collection and refinement statistics for **42**; evaluation of Mcl-1 inhibitors in proliferation assay in cell line panel, comparison to MS-1 activity; additional data for dosing **42** in HCC-1187 xenograft model; additional data for co-dosing experiments with **42** in HCC-1187 xenograft model; screening of compounds **35**−**43** in Mcl-1 sensitive cell line panel; HPLC−MS traces for compounds **6**−**43** (PDF)

Molecular formula strings (CSV)

Accession Codes

PDB code for **1** is 6BW2; PDB code for **42** is 6NE5. Authors will release the atomic coordinates and experimental data upon article publication.

■ AUTHOR INFORMATION

Corresponding Author

*E-mail: stephen.fesik@vanderbilt.edu.

ORCID

Stephen W. Fesik: 0000-0001-5957-6192

Present Addresses

◆Broad Institute, Cambridge, Massachusetts 02412, United States (S.S.).

¶AbbVie, North Chicago, Illinois 60064, United States (Z.B.).

⋈Bristol-Myers-Squibb, Princeton, New Jersey 08540, United States (M.D.M.).

⋈UT Southwestern Medical Center, Dallas, Texas 75390, United States (K.-m.L. and C.L.A.).

⧖University of Arkansas Medical School, Little Rock, Arkansas 72205, United States (B.K.).

●University of Wisconsin, Madison, Wisconsin 53706, United States (S.A.F.).

Notes

The authors declare the following competing financial interest(s): M. R. Savona receives research funding from Astex, Boehringer Ingelheim, Celgene, Incyte, Millennium, Sunesis, and TG Therapeutics, is a consultant/advisory board member for Celgene, Incyte, and Karyopharm, and has equity in Karyopharm. S. W. Fesik receives research funding from Boehringer Ingelheim.

■ ACKNOWLEDGMENTS

The authors thank co-workers at the High-Throughput Screening Core facility of Vanderbilt University, TN, for compound management. This project has been funded in whole or in part with federal funds from the National Cancer

DOI: 10.1021/acs.jmedchem.8b01991
J. Med. Chem. 2019, 62, 3971−3988

Institute, National Institutes of Health, under Chemical Biology Consortium Contract No. HHSN261200800001E. The content of this publication does neither necessarily reflect the views or policies of the Department of Health and Human Services, nor does mention of trade names, commercial products, or organizations imply endorsement by the U.S. Government and a career development award to S.W.F. from a NCI SPORE grant in breast cancer (Grant P50CA098131) to C.L.A. Use of the Advanced Photon Source was supported by the U.S. Department of Energy, Office of Science, Office of Basic Energy Sciences, under Contract No. DE-AC02-06CH11357. A portion of the experiments described here used the Vanderbilt PacVan biomolecular robotic crystallization facility, which was supported by National Institutes of Health Grant S10 RR026915. E. P. Evans Foundation Discovery Research Grant, the Adventure Allie Discovery Research Grant, and the Biff Ruttenberg Foundation to M.R.S. The Vanderbilt-Ingram Cancer Center is supported by a NIH P30 CA068485-19. Authors acknowledge the Vanderbilt-Ingram Cancer Center Hematopoietic Malignancies Tissue Repository. Flow cytometry experiments were performed in the VMC Flow Cytometry Shared Resource. The VMC Flow Cytometry Shared Resource is supported by the Vanderbilt-Ingram Cancer Center (P30 CA68485) and the Vanderbilt Digestive Disease Research Center (DK058404).

■ ABBREVIATIONS

Mcl-1, myeloid cell leukemia 1; BIM, Bcl-2 interacting mediator of cell death; AML, acute myeloid leukemia; BH3, Bcl-2 homology 3; TNBC, triple negative breast cancer

■ REFERENCES

(1) Adams, J. M.; Cory, S. The Bcl-2 Apoptotic Switch in Cancer Development and Therapy. *Oncogene* **2007**, *26*, 1324−1337.
(2) Czabotar, P. E.; Lessene, G.; Strasser, A.; Adams, J. M. Control of Apoptosis by the Bcl-2 Protein Family: Implications for Physiology and Therapy. *Nat. Rev. Mol. Cell Biol.* **2014**, *15*, 49−63.
(3) Hanahan, D.; Weinberg, R. A. The Hallmarks of Cancer. *Cell* **2000**, *100*, 57−70.
(4) Placzek, W. J.; Wei, J.; Kitada, S.; Zhai, D.; Reed, J. C.; Pellecchia, M. A Survey of the Anti-Apoptotic Bcl-2 Subfamily Expression in Cancer Types Provides a Platform to Predict Efficacy of the BCl-2 Antagonists in Cancer Therapy. *Cell Death Dis.* **2010**, *1*, No. e40.
(5) Danial, N. N.; Korsmeyer, S. J. Cell Death: Critical Control Points. *Cell* **2004**, *116*, 205−219.
(6) Reed, J. C. Bcl-2 and the Regulation of Programmed Cell Death. *J. Cell Biol.* **1994**, *124*, 1−6.
(7) Kitanaka, C.; Namiki, T.; Noguchi, K.; Mochizuki, T.; Kagaya, S.; Chi, S.; Hayashi, A.; Asai, A.; Tsujimoto, Y.; Kuchino, Y. Caspase-Dependent Apoptosis of COS-7 Cells Induced by Bax Overexpression: Differential Effects of Bcl-2 and Bcl-xL on Bax-Induced Caspase Activation and Apoptosis. *Oncogene* **1997**, *15*, 1763−1772.
(8) Vogler, M.; Dinsdale, D.; Dyer, M. J.; Cohen, G. M. Bcl-2 Inhibitors: Small Molecules with a Big Impact on Cancer Therapy. *Cell Death Differ.* **2009**, *16*, 360−367.
(9) Beroukhim, R.; Mermel, C. H.; Porter, D.; Wei, G.; Raychaudhuri, S.; Donovan, J.; Barretine, J.; Boehm, J. S.; Dobson, J.; Urashima, M.; McHenry, K. T.; Pinchback, R. M.; Ligon, A. H.; Cho, Y. J.; Haery, L.; Greulich, H.; Reich, M.; Winckler, W.; Lawrence, M. S.; Weir, B. A.; Tanaka, K. E.; Chiang, D. Y.; Bass, A. J.; Loo, A.; Hoffman, C.; Presner, J.; Liefeld, T.; Gao, Q.; Yecis, D.; Signoretti, S.; Maher, E.; Kaye, F. J.; Sadaki, H.; Tepper, J. E.; Fletcher, J. A.; Tabernero, J.; Baselga, J.; Tsao, M. S.; Demichelis, F.; Rubin, M. A.; Janne, P. A.; Daly, M. J.; Nucera, C.; Levine, R. L.; Ebert, B. L.; Gabriel, S.; Rustgi, A. K.; Antonescu, C. R.; Ladanyi, M.; Letai, A.; Garraway, L. A.; Loda, M.; Beer, D. G.; True, L. D.; Okamoto, A.; Pomeroy, S. L.; Singer, S.; Golub, T. R.; Lander, E. S.; Getz, G.; Sellers, W. R.; Meyerson, M. The Landscape of Somatic Copy Number Alteration Across Human Cancers. *Nature* **2010**, *463*, 899−905.
(10) Wei, G.; Margolin, A. A.; Haery, L.; Brown, E.; Cucolo, L.; Julian, B.; Shehata, S.; Kung, A. L.; Beroukhim, R.; Golub, T. R. Chemical Genomics Identifies Small-Molecule MCL1 Repressors and BCL-xL as a Predictor of MCL1 Dependency. *Cancer Cell* **2012**, *21*, 547−562.
(11) Song, L.; Coppola, D.; Livingston, S.; Cress, D.; Haura, E. B. Mcl-1 Regulates Survival and Sensitivity to Diverse Apoptotic Stimuli in Human Non-Small Cell Lung Cancer Cells. *Cancer Biol. Ther.* **2005**, *4*, 267−276.
(12) Ding, Q.; He, X.; Xia, W.; Hsu, J.-M.; Chen, C.-T.; Li, L.-Y.; Lee, D.-F.; Yang, J.-Y.; Xie, X.; Liu, J.-C.; Hung, M.-C. Myeloid Cell Leukemia-1 Inversely Correlates with Glycogen Synthase Kinase-3beta Activity and Associates with Poor Prognosis in Human Breast Cancer. *Cancer Res.* **2007**, *67*, 4564−4571.
(13) Krajewska, M.; Krajewski, S.; Epstein, J. I.; Shabaik, A.; Sauvageot, J.; Song, K.; Kitada, S.; Reed, J. C. Immunohistochemical Analysis of Bcl-2, Bax, Bcl-x, and Mcl-1 Expression in Prostate Cancers. *Am. J. Pathol.* **1996**, *148*, 1567−1576.
(14) Miyamoto, Y.; Hosotani, R.; Wada, M.; Lee, J. U.; Koshiba, T.; Fujimoto, K.; Tsuji, S.; Nakajima, S.; Doi, R.; Kato, M.; Shimada, Y.; Imamura, M. Immunohistochemical Analysis of Bcl-2, Bax, Bcl-X, and Mcl-1 Expression in Pancreatic Cancers. *Oncology* **1999**, *56*, 73−82.
(15) Brotin, E.; Meryet-Figuière, M.; Simonin, K.; Duval, R. E.; Villedieu, M.; Leroy-Dudal, J.; Saison-Behmoaras, E.; Gauduchon, P.; Denoyelle, C.; Poulain, L. Bcl-xL and MCL-1 Constitute Pertinent Targets in Ovarian Carcinoma and Their Concomitant Inhibition is Sufficient to Induce Apoptosis. *Int. J. Cancer* **2010**, *126*, 885−895.
(16) Derenne, S.; Monia, B.; Dean, N. M.; Taylor, J. K.; Rapp, M.-J.; Harousseau, J.-L.; Bataille, R.; Amiot, M. Antisense Strategy Shows that Mcl-1 Rather than Bcl-2 or Bcl-xL is an Essential Survival Protein of Human Myeloma Cells. *Blood* **2002**, *100*, 194−199.
(17) Andersen, M. H.; Becker, J. C.; Thor Straten, P. The Antiapoptotic Member of the Bcl-2 Family Mcl-1 is a CTL Target In Cancer Patients. *Leukemia* **2005**, *19*, 484−485.
(18) Kang, M. H.; Wan, Z.; Kang, Y. H.; Sposto, R.; Reynolds, C. P. Mechanism Of Synergy Of N-(4-Hydroxyphenyl)Retinamide and ABT-737 in Acute Lymphoblastic Leukemia Cell Lines: Mcl-1 Inactivation. *JNCI, J. Natl. Cancer Inst.* **2008**, *100*, 580−595.
(19) Wertz, I. E.; Kusam, S.; Lam, C.; Okamoto, T.; Sandoval, W.; Anderson, D. J.; Helgason, E.; Ernst, J. A.; Eby, M.; Liu, J.; Belmont, L. D.; Kaminker, J. S.; O'Rourke, K. M.; Pujara, K.; Kohli, P. B.; Johnson, A. R.; Chiu, M. L.; Lill, J. R.; Jackson, P. K.; Fairbrother, W. J.; Seshagiri, S.; Ludlam, M. J.; Leong, K. G.; Dueber, E. C.; Maecker, H.; Huang, D. C.; Dixit, V. M. Sensitivity to Antitubulin Chemotherapeutics is Regulated by Mcl-1 And FBW7. *Nature* **2011**, *471*, 110−114.
(20) Wei, S. H.; Dong, K.; Lin, F.; Wang, X.; Li, B.; Shen, J. J.; Zhang, Q.; Wang, R.; Zhang, H. Z. Inducing Apoptosis and Enhancing Chemoselectivity to Gemcitabine via RNA Interference Targeting Mcl-1 Gene in Pancreatic Carcinoma Cell. *Cancer Chemother. Pharmacol.* **2008**, *62*, 1055−1064.
(21) Delbridge, A. R.; Strasser, A. The BCL-2 Protein Family, BH3-Mimetics, and Cancer Therapy. *Cell Death Differ.* **2015**, *22*, 1071−1080.
(22) Liang, H.; Fesik, S. W. Three-Dimensional Structures of Proteins Involved in Programmed Cell Death. *J. Mol. Biol.* **1997**, *274*, 291−302.
(23) Petros, A. M.; Olejniczak, E. T.; Fesik, S. W. Structural Biology of the Bcl-2 Family of Proteins. *Biochim. Biophys. Acta, Mol. Cell Res.* **2004**, *1644*, 83−94.
(24) Stewart, M. L.; Fire, E.; Keating, A. E.; Walensky, L. D. The MCL-1 BH3 Helix is an Exclusive MCL-1 Inhibitor and Apoptosis Sensitizer. *Nat. Chem. Biol.* **2010**, *6*, 595−601.

DOI: 10.1021/acs.jmedchem.8b01991
J. Med. Chem. 2019, 62, 3971−3988

(25) Czabotar, P. E.; Lee, E. F.; van Delft, M. F.; Day, C. L.; Smith, B. J.; Huang, D. C.; Fairlie, W. D.; Hinds, M. G.; Colman, P. M. Structural Insights into the Degradation of Mcl-1 Induced by BH3 Domains. *Proc. Natl. Acad. Sci. U.S.A.* **2007**, *104*, 6217−6222.
(26) Arkin, M. R.; Wells, J. A. Small-Molecule Inhibitors of Protein-Protein Interactions: Progressing Towards the Dream. *Nat. Rev. Drug Discovery* **2004**, *3*, 301−317.
(27) Wendt, M. D. The Discovery of Navitoclax, a Bcl-2 Family Inhibitor. In *Protein−Protein Interactions*; Topics in Medicinal Chemistry; Springer-Verlag: Berlin, Heidelberg, 2012; Vol. *8*, pp 231−258.
(28) Kaefer, A.; Yang, J.; Noertersheuser, P.; Mensing, S.; Humerickhouse, R.; Awni, W.; Xiong, H. Mechanism-Based Pharmacokinetic/Pharmacodynamic Meta-Analysis of Navitoclax (ABT-263) Induced Thrombocytopenia. *Cancer Chemother. Pharmacol.* **2014**, *74*, 593−602.
(29) Souers, A. J.; Leverson, J. D.; Boghaert, E. R.; Ackler, S. L.; Catron, N. D.; Chen, J.; Dayton, B. D.; Ding, H.; Enschede, S. H.; Fairborther, W. J.; Huang, D. C.; Hymowitz, S. G.; Jin, S.; Khaw, S. L.; Kovar, P. J.; Lam, L. T.; Lee, J.; Maecker, H. L.; Marsh, K. C.; Mason, K. D.; Mitten, M. J.; Nimmer, P. M.; Oleksijew, A.; Park, C. H.; Park, C. M.; Phillips, D. C.; Roberts, A. W.; Sampath, D.; Seymour, J. F.; Smith, M. L.; Sullivan, G. M.; Tahir, S. K.; Tse, C.; Wendt, M. D.; Xiao, Y.; Xue, J. C.; Zhang, H.; Humerickhouse, R. A.; Rosenberg, S. H.; Elmore, S. W. ABT-199, a Potent and Selective BCL-2 Inhibitor, Achieves Antitumor Activity While Sparing Platelets. *Nat. Med.* **2013**, *19*, 202−208.
(30) U.S. FDA News Release (April 11, 2016).
(31) Kotschy, A.; Szlavik, Z.; Csekel, M.; Paczal, A.; Szabo, Z.; Sipos, S.; Radics, G.; Proszenyak, A.; Balint, B.; Bruno, A.; Geneste, O.; Davidson, J. E. P.; Murray, J. B.; Chen, I.; Perron-Sierra, F. New Thienopyrimidine Derivative, a Process for Their Preparation and Pharmaceutical Compositions Containing Them. European Patent Application EP2886545A12015.
(32) Szlavik, Z.; Balint, B.; Kotschy, A.; Chanrion, M.; Geneste, O.; Davidson, J. E. P.; Murray, J. B.; Sipos, S.; Proszenyak, A. New Hydroxyacid Derivatives, a Process for Their Preparation and Pharmaceutical Compositions Containing Them. PCT International Application WO2016207216A1, 2016.
(33) Szlavik, Z.; Kotschy, A.; Chanrion, M.; Marles, D.; Geneste, O.; Davidson, J. E. P.; Murray, J. B.; Sipos, S.; Paczal, A.; Balint, B. New Hydroxyester Derivatives, a Process for Their Preparation and Pharmaceutical Compositions Containing Them. PCT International Application WO2016207225A12016.
(34) Szlavik, Z.; Szabo, Z.; Csekel, M.; Paczul, A.; Kotschy, A.; Bruno, A.; Geneste, O.; Chen, I.; Davidson, J. E. P.; Murray, J. B.; Ondi, L.; Radics, G.; Sipos, S.; Proszenyak, A.; Perran-Sierra, F.; Balint, B. New Aminoacid Derivatives, a Process for Their Preparation and Pharmaceutical Compositions Containing Them. PCT International Application WO2016207226A12016.
(35) Brown, S. P.; Li, Y.; Lizarzaburu, M. E.; Lucas, B. S.; Paras, N. A.; Taygerly, J.; Vimolratana, M.; Wang, X.; Yu, M.; Zancanella, M.; Zhu, L.; Buenrostro, A. G.; Li, Z. Tetrahydronaphthalene Derivatives that Inhibit Mcl-1 Protein. PCT International Application WO2016033486, 2016.
(36) Johannes, J. W.; Bates, S.; Beigie, C.; Belmonte, M. A.; Breen, J.; Cao, S.; Centrella, P. A.; Clark, M. A.; Cuozzo, J. W.; Dumelin, C. E.; Ferguson, A. D.; Habeshian, S.; Hargreaves, D.; Joubran, C.; Kazmirski, S.; Keefe, A. D.; Lamb, M. L.; Lan, H.; Li, Y.; Ma, H.; Mlynarski, S.; Packer, M. J.; Rawlins, P. B.; Robbins, D. W.; Shen, H.; Sigel, E. A.; Soutter, H. H.; Su, N.; Troast, D. M.; Wang, H.; Wickson, K. F.; Wu, C.; Zhang, Y.; Zhao, Q.; Zheng, X.; Hird, A. W. Structure Based Design of Non-Natural Peptidic Macrocyclic Mcl-1 Inhibitors. *ACS Med. Chem. Lett.* **2017**, *8*, 239−244.
(37) Hird, A.; Yang, W.; Robbins, D.; Kazmirski, S.; Wu, D.; Peng, B.; Johannes, J.; Lamb, M. MCL-1 Inhibitors and Methods of Use Thereof. US20170305926A1, 2017.
(38) Kotschy, A.; Szlavik, Z.; Murray, J.; Davidson, J.; Maragno, A. L.; Le Toumelin-Braizat, G.; Chanrion, M.; Kelly, G. L.; Gong, J.; Moujalled, D. M.; Bruno, A.; Csekei, M.; Paczal, A.; Szable, Z. B.; Sipos, S.; Radics, G.; Proszenyak, A.; Balint, B.; Ondi, L.; Blasko, G.; Robertson, A.; Surgenor, A.; Dokurno, P.; Chen, I.; Matassova, N.; Smith, J.; Pedder, C.; Graham, C.; Studney, A.; Lysiak-Auvity, G.; Girard, A.; Grave, F.; Segal, D.; Riffkin, C. D.; Pomilio, G.; Galbraith, L. C. A.; Aubrey, B. J.; Brennan, M. S.; Herold, M. J.; Chang, C.; Guasconi, G.; Cauquil, N.; Melchiore, F.; Guigal-Stephan, N.; Lockhart, B.; Colland, F.; Hickman, J. A.; Roberts, A. W.; Huang, D. C. S.; Wei, A. H.; Strasser, A.; Lessene, G.; Geneste, O. The Mcl1 Inhibitor S63845 is Tolerable and Effective in Diverse Cancer Models. *Nature* **2016**, *538*, 477−482.
(39) Shaw, S.; Bian, Z.; Zhao, B.; Tarr, J. C.; Veerasamy, N.; Jeon, K. O.; Belmar, J.; Arnold, A. L.; Fogarty, S. A.; Perry, E.; Sensintaffar, J. L.; Camper, D. V.; Rossanese, O. W.; Lee, T.; Olejniczak, E. T.; Fesik, S. W. Optimization of Potent and Selective Tricyclic Indole Diazepinone Myeloid Cell Leukemia-1 Inhibitors Using Structure-Based Design. *J. Med. Chem.* **2018**, *61*, 2410−2421.
(40) Friberg, A.; Vigil, D.; Zhao, B.; Daniels, R. N.; Burke, J. P.; Garcia-Barrantes, P. M.; Camper, D.; Chauder, B. A.; Lee, T.; Olejniczak, E. T.; Fesik, S. W. Discovery of Potent Myeloid Cell Leukemia 1 (Mcl-1) Inhibitors Using Fragment-Based Methods and Structure-Based Design. *J. Med. Chem.* **2013**, *56*, 15−30.
(41) Burke, J. P.; Bian, Z.; Shaw, S.; Zhao, B.; Goodwin, C. M.; Belmar, J.; Browning, C. F.; Vigil, D.; Friberg, A.; Camper, D. V.; Rossanese, O. W.; Lee, T.; Olejniczak, E. T.; Fesik, S. W. Discovery of Tricyclic Indoles that Potently Inhibit Mcl-1 Using Fragment-Based Methods and Structure-Based Design. *J. Med. Chem.* **2015**, *58*, 3794−3805.
(42) Pelz, N. F.; Bian, Z.; Zhao, B.; Shaw, S.; Tarr, J. C.; Belmar, J.; Gregg, C.; Camper, D. V.; Goodwin, C. M.; Arnold, A. L.; Sensintaffar, J. L.; Friberg, A.; Rossanese, O. W.; Lee, T.; Olejniczak, E. T.; Fesik, S. W. Discovery of 2-Indole-acylsulfonamide Myeloid Cell Leukemia 1 (Mcl-1) Inhibitors Using Fragment-Based Methods. *J. Med. Chem.* **2016**, *59*, 2054−2066.
(43) Lee, T.; Bian, Z.; Zhao, B.; Hogdal, L. J.; Sensintaffar, J. L.; Goodwin, C. M.; Belmar, J.; Shaw, S.; Tarr, J. C.; Veerasamy, N.; Matulis, S. M.; Koss, B.; Fischer, M. A.; Arnold, A. L.; Camper, D. V.; Browning, C. F.; Rossanese, O. W.; Budhraja, A.; Opferman, J.; Boise, L. H.; Savona, M. R.; Letai, A.; Olejniczak, E. T.; Fesik, S. W. Discovery and Biological Characterization of Potent Myeloid Cell Leukemia-1 Inhibitors. *FEBS Lett.* **2017**, *591*, 240−251.
(44) Ramsey, H. E.; Fischer, M. A.; Lee, T.; Gorska, A. E.; Arrate, M. P.; Fuller, L.; Boyd, K.; Strickland, S. A.; Sensintaffar, J.; Hogdal, L.; Ayers, G. D.; Olejniczak, E. T.; Fesik, S. W.; Savona, M. R. A Novel MCL-1 Inhibitor Combined with Venetoclax Resucues Venetoclax Resistant Acute Myelogenous Leukemia. *Cancer Discovery* **2018**, *8*, 1566−1581.
(45) Foicht, G. W.; Ryan, J. A.; Gullá, S. V.; Letai, A.; Keating, A. E. Designed BH3 Peptides with High Affinity and Specificity for Targeting Mcl-1 in Cells. *ACS Chem. Biol.* **2014**, *9*, 1962−1968.
(46) Koss, B.; Morrison, J.; Perciavalle, R. M.; Singh, H.; Rehg, J. E.; Williams, R. T.; Opferman, J. T. Requirements for Antiapoptotic MCL-1 in the Survival of BCR-ABL B-lineage Acute Lymphoblastic Leukemia. *Blood* **2013**, *122*, 1587−1598.
(47) Opferman, J. T.; Letai, A.; Beard, C.; Sorcinelli, M. D.; Ong, C. C.; Korsmeyer, S. J. Development and Maintenance of B and T Lymphocytes Requires Antiapoptotic MCL-1. *Nature* **2003**, *426*, 671−676.
(48) Takeuchi, O.; Fisher, J.; Suh, H.; Harada, H.; Malynn, B. A.; Korsmeyer, S. J. Essential Role of BAX, BAK in B Cell Homeostasis and Prevention of Autoimmune Disease. *Proc. Natl. Acad. Sci. U.S.A.* **2005**, *102*, 11272−11277.
(49) Kamijo, T.; Zindy, F.; Roussel, M. F.; Quelle, D. E.; Downing, J. R.; Ashmun, R. A.; Grosveld, G.; Sherr, C. J. Tumor Suppression at the Mouse INK4a Locus Mediated by the Alternative Reading Frame Product p19ARF. *Cell* **1997**, *91*, 649−659.
(50) Koss, B.; Ryan, J.; Budhraja, A.; Szarama, K.; Yang, X.; Bathina, M.; Cardone, M. H.; Nikolovska-Coleska, Z.; Letai, A.; Opferman, J. T. Defining Specificity and On-Target Activity of BH3-Mimetics

DOI: 10.1021/acs.jmedchem.8b01991
J. Med. Chem. 2019, 62, 3971−3988

Using Engineered B-ALL Cell Lines. *Oncotarget* **2016**, *7*, 11500−11511.
(51) Wahba, H. A.; El-Hadaad, H. A. Current Approaches in Treatment of Triple Negative Breast Cancer. *Cancer Biol. Med.* **2015**, *12*, 106−116.
(52) Otwinowski, Z.; Minor, W. Processing of X-ray Diffraction Data Collected in Oscillation Mode. In *Methods in Enzymology*; Carter, C. W., Jr., Sweet, R. M, Eds.; Macromolecular Crystallography Part A; Academic Press: San Diego, CA, 1997; Vol. *276*, pp 307−326.
(53) McCoy, A. J.; Grosse-Kunstleve, R. W.; Adams, P. D.; Winn, M. D.; Storoni, L. C.; Read, R. J. Phaser Crystallographic Software. *J. Appl. Crystallogr.* **2007**, *40*, 658−674.
(54) Collaborative Computational Project, Number 4. The CCP4 Suite: Programs for Protein Crystallography. *Acta Crystallogr., Sect. D: Biol. Crystallogr.* **1994**, *50*, 760−763.
(55) Emsley, P.; Cowtan, K. Coot: Model-Building Tools for Molecular Graphics. *Acta Crystallogr., Sect. D: Biol. Crystallogr.* **2004**, *60*, 2126−2132.
(56) Nikolovska-Coleska, Z.; Wang, R.; Fang, X.; Pan, H.; Tomita, Y.; Li, P.; Roller, P. P.; Krajewski, K.; Saito, N. G.; Stuckey, J. A.; Wang, S. Development and Optimization of a Binding Assay for the XIAP BIR3 Domain Using Fluorescence Polarization. *Anal. Biochem.* **2004**, *332*, 261−273.

DOI: 10.1021/acs.jmedchem.8b01991
J. Med. Chem. 2019, 62, 3971−3988